Lappeenranta University of Technology
School of Energy Systems
Master`s Degree Programme in Electrical Engineering

Aleksandr Mirlenko

CONTROL OF ELECTRICALLY EXCITED SYNCHRONOUS MOTOR IN THE FIELD WEAKENING RANGE

Examiners: Professor Olli Pyrhönen

Supervisors: Professor Olli Pyrhönen
Researcher, D.Sc. Pasi Peltoniemi

ABSTRACT

Lappeenranta University of Technology
School of Energy Systems
Master`s Degree Programme in Electrical Engineering

Aleksandr Mirlenko

Control of electrically excited synchronous motor in the field weakening range

Master's Thesis

2017

63 pages, 28 figures, 2 tables

Examiners: Professor Olli Pyrhönen

Keywords: Synchronous motor, field oriented control, field weakening, reaction control, flux linkage estimator, robustness.

In the current thesis, the control system for the electrically excited synchronous motor is investigated. The main topics within the work are field oriented control, field weakening, reaction control, robustness. The field weakening technique is used to increase the motor operational speed range to the limit of double nominal speed; in the control system field weakening is implemented as a flux limiter. Two different excitation control principles are studied: unity power factor control and reaction control; their impact on the drive performance is investigated, and the results are compared. The stator flux linkage reference vector, the stator current controllers tuning, and the torque load rise time are the drive tuning parameters researched. To enhance the drive robustness, the voltage model based estimator with the current model based correction term is implemented. During the simulations in MATLAB Simulink, the drive dynamic performance, as well as the robustness to the internal disturbances was tested. The results obtained justified the control system efficiency in dynamic performance.

Acknowledgements

The current thesis was carried out at School of Energy Systems, Lappeenranta University of Technology.

I would like to express my sincere gratitude to Professor Olli Pyrhönen, and Researcher D.Sc. Pasi Peltoniemi, the master`s thesis supervisors for their invaluable help throughout the research. The project would be impossible to accomplish without your support and encouragement. Thank you!

I would like to thank D.Sc. Victor Vtorov from Saint Petersburg Electrotechnical University "LETI" for his significant help in managing all the issues concerning the double degree programme. I also wish to thank Maria Kiseleva, Director of International Academic Mobility Office, who made the double degree programme possible.

I am immensely obliged to my brother Pavel Mirlenko for his advice and encouragement 24/7. Your opinion is always important to me.

My parents deserve special thanks for their love and support. You have been providing me with all the best you have throughout my entire life.

Lappeenranta, August 2017 Aleksandr Mirlenko

List of abbreviations and symbols

emf	electromotive force
pu	per unit values
AC	alternating current
DC	direct current
DTC	direct torque control
EESM	electrically excited SM
FOC	field oriented control
IM	induction motor
PF	power factor
PI	proportional-integral
PWM	pulse-width modulation
SM	synchronous motor
SVPWM	space vector PWM
VSI	voltage source inverter

TABLE OF CONTENTS

1. INTRODUCTION

Synchronous motors are commonly used in both fixed and variable speed drives. Among industrial applications, where the motor is supposed to be driven at a constant speed level, are centrifugal and reciprocating pumps, compressors, fans, wood grinders and refiners.
Applications requiring variable speed operations are mine hoists, rolling mills, and propulsion systems; in case of applications in ventilation and pumping systems variable speed synchronous drives provide significant energy savings [17]. Due to their ability to change power factor, synchronous motors are also often used for power factor correction in electrical power systems [1].
Undoubted benefit of synchronous motors in comparison with induction ones is the fact that the excitation from a separate DC source allows the motor to operate at high power factor values, both leading and lagging ones. This feature makes the power factor correction of the whole electrical system possible. High $\cos(\phi)$ value also provides the consumed current reduction and the losses reduction. SM has higher overload ability, what makes them reliable and safe. Among the drawbacks of SM is the design complexity leading to the production cost increase. Besides that, the SM start is also a more complex process than the IM start. However, from the SM applications it can be seen, that nowadays they are irreplaceable in the long-term constant speed and load technological processes, where the frequent start/stop operations are not required [17].
Synchronous machines can be divided into two main types: non-excited and DC-excited machines. In DC-excited motors the flux control is implemented easier than in non-excited ones, e.g. permanent magnet synchronous machines, that require more complicated control algorithms to be driven into the field weakening range.
In the current work, the electrically excited synchronous machine performance in the field weakening range is investigated. Basic concepts of the EESM are presented in the next paragraph.

1.1 Electrically excited synchronous motor

A synchronous motor is a type of AC electrical machines. As its name suggests, in steady state the rotor rotation is synchronous with the magnetic field, that the armature winding causes to rotate.

There exist different types of synchronous machines: separately magnetized SM, reluctance SM, permanent magnet SM, and their combinations. The further classification divides the aforementioned machines in salient pole and non-salient pole in accordance with the rotor type, and with brushes and brushless in accordance with the rotor excitation method.

The motor used for the vector control performance investigation in the field weakening range studied within the current work is of a separately magnetized type. Electrically excited synchronous motor is a type of DC-excited synchronous machine with rotor windings. The presence of the rotor windings is reflected in another name of such machine – wound rotor synchronous motor that is commonly used in the U.S. Thus, the field winding current, also called excitation current, can also be a controlled variable in a separately magnetized SM drives.

The investigated in the current work EESM has the rotor implemented in a salient-pole type. The rotor winding is placed around the magnetic poles iron core. The magnetic poles themselves are placed on the rotor shaft. The poles outer surface carries a damper winding that are used to delay the air-gap flux change rate and accelerate the stator current change rate, what makes the machine torque change more rapidly. This design feature allows to improve the drive stability and dynamic performance. Figure 1.1 illustrates the salient-pole synchronous machine rotor and stator, as well as the space vector diagram [1].

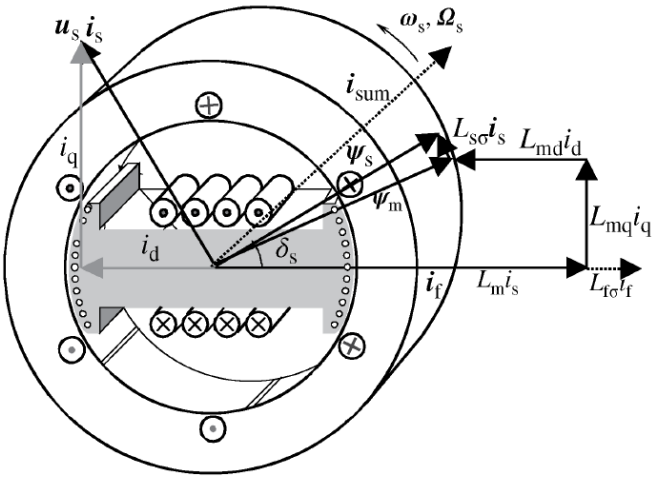

Figure 1.1 – Salient-pole machine space-vector diagram. Source: [1].

In Figure 1.1, the following denominations are used: $\boldsymbol{u}_s$, $\boldsymbol{i}_s$ – stator voltage and current respectively; $\boldsymbol{i}_f$ – field winding (excitation) current; $\boldsymbol{i}_{sum}$ – current vectors sum; $\boldsymbol{\psi}_s$, $\boldsymbol{\psi}_m$ –

stator and air-gap flux linkage respectively; $\boldsymbol{\omega}_s$, $\boldsymbol{\Omega}_s$ – electrical and mechanical angular velocities.

The magnetic poles mounted on the rotor are magnetically locked with the magnetic field in the air-gap; the rotation rate of the magnetic field is synchronous with the supply voltage frequency.

Salient-pole machines have better cooling because of the rotor shape dimensions [1]. However, such a synchronous motor configuration has magnetic anisotropy in the cross section and complicated saturation phenomena.

Synchronous motors are widely used in different industries. In rolling mill and steel- industry SMs are used as roller drives, both main and auxiliary. In cement industry among possible applications are fans and mills, as well as rotary kilns. Chemical, oil, and gas industries are also in need of synchronous motor drives, used for compressors, extruders, and fans. In manufacturing industry, the pulp grinders are one of possible application of SMs. In power plant technology, pumps can be driven by synchronous motors [18].

High-power synchronous motors can bring a benefit of power factor correction. SMs can also be used as electrical vehicle traction motors, e.g. TGV trains (France) are constructed based on synchronous motor drives [1].

1.2 Vector control

The main contemporary control techniques for AC electrical motors are direct torque control (DTC), direct flux linkage control (DFLC), and field oriented control (FOC) – the method studied in the current work. All the principles mentioned are based on the idea to accurately estimate and drive the machine electromagnetic state.

In accordance with the FOC principle, the synchronous motor control is simplified to the DC motors control principles, what makes control algorithms easier and less time consuming while carried out [1]. In field oriented control, flux linkage and torque required are obtained by controlling the stator and excitation currents.

The idea behind the EESM vector control is to specify the stator and field winding currents reference vectors in such a way, so that the motor torque and excitation are controlled separately and at any time instant both in steady state, including field weakening range, and during transients. Thus, the reference vectors mentioned should be specified independently: one is responsible for producing torque required (the $\boldsymbol{i}_{\mathrm{T}}$ current component); the other is

used to produce the flux linkage (the $\boldsymbol{i}_{\psi}$ current component). For this reason, the special reference frame with one of the axis (ψ-axis) being aligned with the air-gap flux linkage is required to specify flux- and torque producing current components ($\boldsymbol{i}_{\psi}$ and $\boldsymbol{i}_{\mathrm{T}}$ respectively) [1]. Thus, one of the objectives behind the vector control principle is to compute the flux and torque producing current components references, based on the speed reference required, and to put these space vectors of the desired length to the positions perpendicular to each other.

The electrical torque produced has the following expression:

$$\boldsymbol{T}_e = \frac{3}{2} p \boldsymbol{\psi}_s \times \boldsymbol{i}_s \,, \tag{1.1}$$

where p is the pole pairs number, $\boldsymbol{\psi}_s$ – stator flux linkage space vector, $\boldsymbol{i}_s$ – stator current space vector.

In accordance with the cross-field principle, the electrical torque reaches its maximum magnitude, when the stator flux linkage and stator current vectors are orthogonal to each other, i.e. the angle between them is 90 electrical degrees. For this reason, the current and flux vectors should be controlled in such a way, so that these vectors are orthogonal to each other. Because the control principle is based on the vectors, its title is vector control. In vector control systems, the machines voltages are calculated based on the currents measured, and the motor state is estimated [1].

The FOC technique main features are:

- control frame transformation;
- equivalent circuit analysis;
- demand for accurate machine inductances values.

Coordinate transformation is used to make the machine control easier. In the FOC technique the control frames used (rotor and stator, also known as field oriented and flux linkage oriented reference frames) rotate at synchronous speed, what allows to control AC variables specified in different coordinate axes as DC quantities, making the motor control algorithms easier, and less laborious and time-consuming. The motor currents are specified in the stator oriented reference frame, also known as the flux linkage oriented control frame (ψT – axes), and in the rotor oriented reference frame, also called the field oriented control frame (dq – axes).

The stator currents and voltages references are calculated by the PI controllers. These vectors are specified in the rotor control frame. However, the voltages supplied to a converter (in the studied case, voltage source inverter) must be specified in the stator reference frame, so coordinate transformation techniques for the control frames conversion are required.

The equivalent circuit analysis is required to accurately estimate the stator flux linkage, and damper currents. In accordance with the machine mathematical model based on the equivalent circuit analysis, the voltage and current models equations are defined. In the FOC method the motor excitation and torque can be controlled independently. This control algorithm requires the voltage model and the current model equations to be written in accordance with the motor equivalent circuit. Precisely measured machine inductances allow to tune the controllers correctly.

The main difference between these control methods is that in DTC the current control loops are not included in the control system. The flux control and the torque control loops are used instead to control the drive in accordance with the principle. The same current model of the machine is suitable for both techniques. Both DTC and FOC algorithms can be used to drive the EESM. Nowadays, the most widespread and contemporary AC machines control method is the vector control; the current work is focused on the FOC implementation.

1.3 Voltage source inverter

Electrical drives comprise not only the motor to be driven, and a custom control system, that defines the drive working process, but also a converter, that supplies the motor with the voltage of the magnitude and frequency required. The variable-frequency converter represents the link between the power source and the driven motor.

In the current work pulse width modulated voltage source inverter (PWM-VSI) is studied.

In the VSI, the input is the DC voltage source. The converter schematic diagram is illustrated in Figure 1.2.

The figure can be described as follows. The switch-mode inverter has a single-phase AC input. The AC voltage supplied to the diode bridge rectifier is converted to the DC voltage, filtered by a DC-bus capacitor, and then is inverted in the PWM-VSI. In pulse-width-modulated converters the DC voltage magnitude is kept constant. The voltage source inverter input is a DC single-phase, while its AC output has three phases. The synchronous motor is

fed with the obtained at the inverter output three-phase voltage of the required magnitude and frequency.

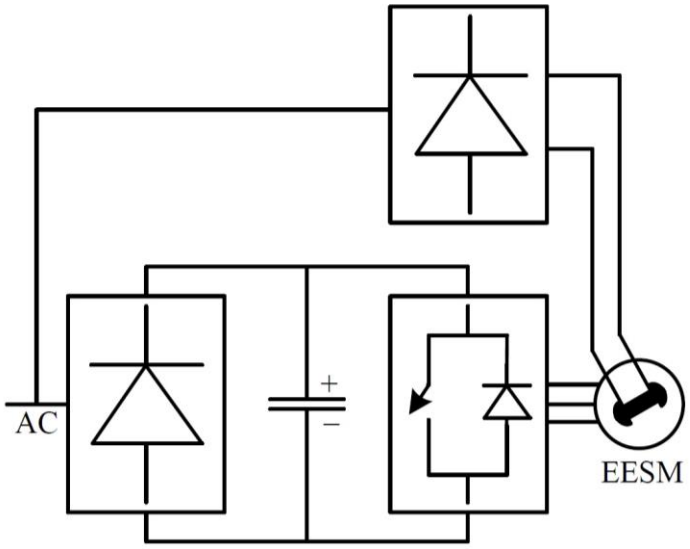

Figure 1.2 – Switch-mode inverter in synchronous motor drive

As a modulation technique, space vector pulse-width modulation (SVPWM) is used. The SVPWM method is a contemporary computation-intensive modulation technique, and provides advanced performance for variable frequency drive applications. One of its major benefits is the total harmonic distortion reduction [17].

1.4 Thesis outline

As the technical task for the current work states, the main topic is the research of the EESM drive control. The studied drive should fulfill the following requirements.

First of all, the studied drive working speed range should be extended to the limit of double rated speed. The operational speed range increase is implemented in accordance with the field weakening technique described in paragraph 2.2. The drive should have high dynamic performance level in the field weakening range.

Secondly, the drive should have high dynamic performance level. The dynamic performance is supposed to be analyzed based on the torque and speed steps obtained during the simulations. The transients after the torque load application are evaluated. Also, the load angle curve is checked to ensure 90° exceeding prevention, i.e. synchronism maintenance.

In case of the reaction control implementation, the power factor curve is analyzed as well. In the field weakening range after the transient the power factor level should coincide with the value specified in the control algorithm.

Finally, the drive robustness in both steady state and field weakening regions should be tested to withstand the internal impacts. In the model the inductances values are assumed to be constant and accurate enough to match the hardware parameters. However, this assumption is not always valid, as the motor inductances can be subject to saturation. The magnetizing inductances can vary within a certain limit while operating in the field weakening range, that is the subject for consideration while designing the control system.

As the main problem and challenges in the work are pointed out clearly, the possible solutions supposed to be analyzed and simulated are presented further.

The field weakening operational range is planned to be implemented by specifying the stator flux linkage reference values. The flux limiter, that is necessary for the field weakening implementation, can be realized by specifying the stator flux linkage reference vector linked together with the corresponding actual angular speed values. Below the rated speed (in the motor used for the current research the rated speed equals 1500 rpm) there is no need in the stator flux linkage reduction. Thus, the values in the flux limiter are equal to unity, i.e. the maximum flux available at the stator. As the drive operational speed goes beyond the rated value limit, the stator flux linkage values are reduced proportionally. The calculation equations and obtained values are presented in further paragraphs.

Another possible solution to the drive implementation is the reaction excitation control principle, introduced by Mård et al. in 1990 [1][2]. The reaction control is applied in the field weakening range, and is used to calculate the excitation current reference. In accordance with the principle, the power factor and the flux producing current component should be set artificially. Both unity and lagging power factor values are tested. The relations between the power factor value, current components, and their impact on the dynamic performance are discussed thoroughly in paragraph 3.4.

The robustness is studied assuming wrong machine parameters. For this reason, the magnetizing inductances are specified considering the saturation phenomena, while the controllers are tuned in accordance with the rated inductances. This technique allows to approximate the simulation to the real-life equipment tests. In order to enhance the drive ability to withstand the saturated magnetizing inductances, the voltage model based estimator is introduced.

The dynamic performance can be adjusted by tuning different parameters. In the current work the focus is on the adjustments of the load torque rise time, and stator current controllers rise time. Two different excitation current reference calculation methods are studied as well: the unity power factor control principle and the reaction control principle. Different combinations of those are simulated in order to find out the most suitable solution to the problem.

As a basis of the work, the already developed EESM drive vector control system has been taken. However, the existing control system has the limited operating speed range, as well as the drive dynamic performance has significant prospects of development. Therefore, the aim of the work is to enhance the EESM drive speed, stability, and robustness performance issues.

The main topics in the work are:

- field oriented control;
- field weakening operation;
- dynamic performance and robustness analysis;
- control system simulation.

The current work can be divided into two main logical parts.

The first logical part, chapter 1-3, presents the introduction into synchronous motors industry applications, and the electrically excited synchronous motor concepts are described briefly. The vector control methods are discussed and compared. In the second chapter the theoretical background related to the research field is used to state the problems, and to present possible solutions. Then, the synchronous motor drive is discussed. The field weakening, i.e. the technique for increasing the motor speed to the levels above the nominal value is introduced. Then, the control system modelling process is presented. Firstly, the synchronous motor drive Simulink model is discretized; the main blocks constituting both the control part and synchronous motor part are described. Finally, in chapter 3, the model adjustments required to achieve the objectives presented in chapter 2 are discussed. All necessary calculations related to the control algorithms are made. The models for the following simulation in Matlab Simulink are presented. The robustness issues are discussed.

In the second logical part, chapter 4, the final simulation models are presented. The results obtained during the simulations are given, analyzed, and compared with the theoretical results; the most suitable solution for the problem stated is recommended to be used for the EESM drive control system implementation.

2. CONTROL SYSTEM MODELLING

In this chapter the EESM control system modelling process is presented.

The drive modelling is impossible without proper understanding of physical processes flowing inside the driven motor. For this reason, the EESM equivalent circuit analysis is conducted, and the voltage and current mathematical models are written.

Then, the drive model overview is presented. As the model basis, the already built model in the Simulink software is used. However, to fulfill the current work requirements, i.e. higher speeds availability due to field weakening, enhanced robustness and dynamic performance, several modifications should be implemented. The model improvements techniques are discussed.

2.1 Synchronous motor drive

The main part of any electrical drive is undoubtedly the motor, that is required to be driven. The motor studied in the current work is the electrically excited synchronous motor discussed in paragraph 1.1.

Any electrical machine can be described using mathematical model, i.e. equations presenting the relation between machine voltages, currents, and flux linkages. To build the EESM model in MATLAB Simulink, the motor voltage model equations are required.

The current mathematical model is used to build the estimator. The estimator allows to calculate (estimate) the motor parameters values, that cannot be measured directly. In the EESM drive model, the parameters needed to be estimated are the damper currents $\boldsymbol{i}_D$ and $\boldsymbol{i}_Q$, the stator, damper winding and magnetizing flux linkages in both axes ($\boldsymbol{\psi}_d$, $\boldsymbol{\psi}_q$, $\boldsymbol{\psi}_D$, $\boldsymbol{\psi}_Q$, $\boldsymbol{\psi}_{md}$, $\boldsymbol{\psi}_{mq}$ respectively). The load angle cosine and sine values are also calculated in accordance with the equations:

$$\cos(\delta_s) = \frac{\boldsymbol{\psi}_d}{\sqrt{(\boldsymbol{\psi}_d^2 + \boldsymbol{\psi}_q^2)}}, \tag{2.1}$$

$$\sin(\delta_s) = \frac{\boldsymbol{\psi}_q}{\sqrt{(\boldsymbol{\psi}_d^2 + \boldsymbol{\psi}_q^2)}} \tag{2.2}$$

The obtained values from the estimator flux linkage are supplied to the stator flux controller and the stator current controller. These low-level controllers are discussed thoroughly in paragraph 2.2.

The motor mathematical models equations mentioned are written based on the machine equivalent circuit. An equivalent circuit is an electrical circuit, in which all real elements are substituted with the corresponding ideal elements (resistors, inductances, capacitors, voltage and current sources).

The EESM equivalent circuit in dq-axes is illustrated in Figure 2.1.

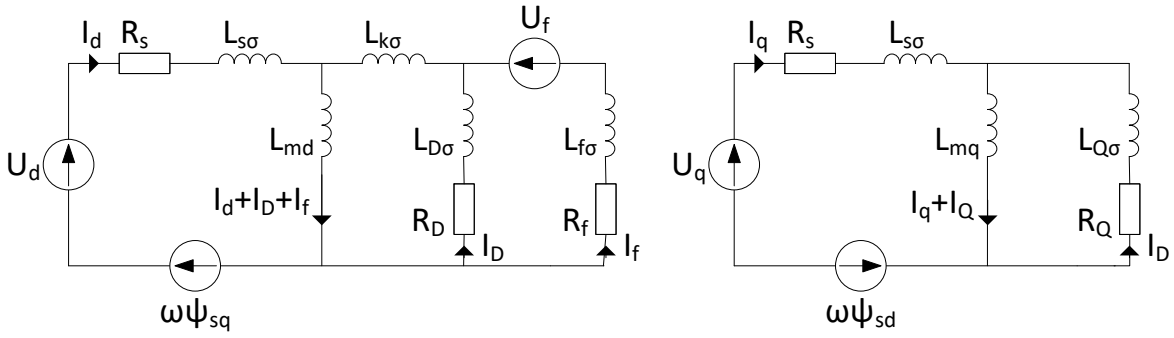

Figure 2.1 – Equivalent circuit of the electrically excited synchronous motor. Source: [2].

In Figure 2.1, the following denominations are used: U_d, U_q – stator voltages in d- and q-axis respectively; I_d, I_q – stator currents in d- and q-axis respectively; I_D, I_Q – rotor currents in d- and q-axis respectively; U_f, i_f – excitation voltage and current respectively; R_s, R_D, R_Q, R_f – stator winding, damper winding in d- and q-axis, field winding resistances respectively; $L_{s\varsigma}$, $L_{D\varsigma}$, $L_{Q\varsigma}$, $L_{f\varsigma}$– stator winding, damper windings in d- and q-axis, field winding stray inductances respectively; L_{md}, L_{mq} – magnetizing inductances in d- and q-axis respectively.

Based on the equivalent circuit, the voltage dq-axes model of the EESM is:

$$\boldsymbol{u}_d = R_s \boldsymbol{i}_d + \frac{d}{dt}\boldsymbol{\psi}_d - \boldsymbol{\omega}\boldsymbol{\psi}_q \,, \tag{2.3}$$

$$\boldsymbol{u}_q = R_s \boldsymbol{i}_q + \frac{d}{dt}\boldsymbol{\psi}_q + \boldsymbol{\omega}\boldsymbol{\psi}_d \,, \tag{2.4}$$

$$0 = R_D \boldsymbol{i}_D + \frac{d}{dt}\boldsymbol{\psi}_D \,, \tag{2.5}$$

$$0 = R_Q \boldsymbol{i}_Q + \frac{d}{dt}\boldsymbol{\psi}_Q \,, \tag{2.6}$$

$$\boldsymbol{u}_f = R_f \boldsymbol{i}_f + \frac{d}{dt}\boldsymbol{\psi}_f \tag{2.7}$$

Equations (2.3 – 2.4) are the expressions of the stator voltage d- and q-parts; the d- and q-axis damper windings are expressed by equations (2.5 – 2.6); the rotor field winding equation is given by formula (2.7). The machine currents can be written as:

$$\boldsymbol{i}_d = \frac{C}{A}\boldsymbol{\psi}_d - \frac{D}{A}\boldsymbol{\psi}_D - \frac{E}{A}\boldsymbol{\psi}_f \,, \tag{2.8}$$

$$\boldsymbol{i}_q = \frac{L_Q}{B}\boldsymbol{\psi}_q - \frac{L_{mq}}{B}\boldsymbol{\psi}_Q \,, \tag{2.9}$$

$$\boldsymbol{i}_D = \frac{F}{A}\boldsymbol{\psi}_D - \frac{H}{A}\boldsymbol{\psi}_f - \frac{D}{A}\boldsymbol{\psi}_d \,, \tag{2.10}$$

$$\boldsymbol{i}_Q = \frac{L_q}{B}\boldsymbol{\psi}_Q - \frac{L_{mq}}{B}\boldsymbol{\psi}_q \,, \tag{2.11}$$

$$\boldsymbol{i}_f = \frac{G}{A}\boldsymbol{\psi}_f - \frac{H}{A}\boldsymbol{\psi}_D - \frac{E}{A}\boldsymbol{\psi}_d \,, \tag{2.12}$$

where $\boldsymbol{\psi}_d$, $\boldsymbol{\psi}_q$ – stator flux linkage in d- and q-axis respectively; $\boldsymbol{\psi}_D$, $\boldsymbol{\psi}_Q$ – damper winding flux linkage in d- and q-axis respectively; $\boldsymbol{\psi}_f$ – field winding flux linkage.

The coefficients in (2.8 - 2.12) are substituted with the calculated inductances:

$$A = L_D L_f L_d - L_{md}^2\left(L_D + L_f + L_d - 2L_{md}\right), \tag{2.13}$$

$$B = L_q L_Q - L_{mq}^2 \,, \tag{2.14}$$

$$C = L_D L_f - L_{md}^2 \,, \tag{2.15}$$

$$D = L_{md} L_f - L_{md}^2 \,, \tag{2.16}$$

$$E = L_{md} L_D - L_{md}^2 \,, \tag{2.17}$$

$$F = L_f L_d - L_{md}^2 \,, \tag{2.18}$$

$$G = L_D L_d - L_{md}^2 \,, \tag{2.19}$$

$$H = L_{md} L_d - L_{md}^2 \,, \tag{2.20}$$

where L_{md} and L_{mq} - d-axis and q-axis magnetizing inductances respectively; L_d and L_D - d-axis stator and rotor inductances respectively; L_q and L_Q - q-axis stator and rotor inductances

respectively; L_f – field (excitation) inductance. The ratio of the inductances in d- and q-axis in salient-pole machines is greater than 1.

The electrically excited synchronous motor current model equations are the following:

$$|\boldsymbol{\psi}_s| = \sqrt{\boldsymbol{\psi}_d^2 + \boldsymbol{\psi}_q^2} \tag{2.21}$$

$$\boldsymbol{\psi}_d = L_{s\sigma}\boldsymbol{i}_d + L_{md}(\boldsymbol{i}_d + \boldsymbol{i}_D + \boldsymbol{i}_f) \tag{2.22}$$

$$\boldsymbol{\psi}_q = L_{s\sigma}\boldsymbol{i}_q + L_{mq}(\boldsymbol{i}_q + \boldsymbol{i}_Q) \tag{2.23}$$

$$\boldsymbol{\psi}_{md} = L_{md}(\boldsymbol{i}_d + \boldsymbol{i}_D + \boldsymbol{i}_f) \tag{2.24}$$

$$\boldsymbol{\psi}_{mq} = L_{mq}(\boldsymbol{i}_q + \boldsymbol{i}_Q) \tag{2.25}$$

The EESM drive control algorithm is based on the field oriented control technique. The signal processing diagram for the EESM drive is illustrated in Figure 2.2.

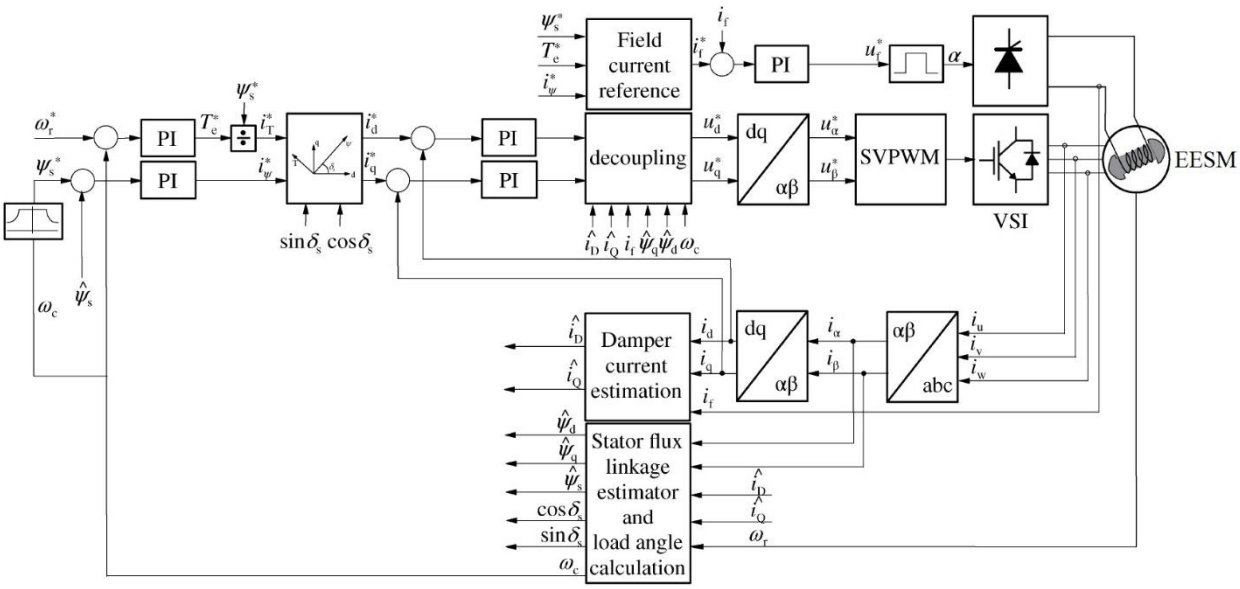

Figure 2.2 – Electrically excited synchronous motor drive functional scheme. Source: [1].

In the FOC method five low-level controllers are used: two controllers for the flux producing and torque producing current components; the stator flux linkage controller; the excitation (field winding current) controller; the speed controller. All the controllers mentioned are based on the proportional-integral (PI) controller. Generally, the error between the reference

and feedback values is supplied to the PI-controller, that generates the control signal. The tuning process and working principle of each controller is presented more specifically in chapter 2.

The ‘field current reference’ block located before the excitation PI controller represents the excitation current reference values calculation method. In the current work the methods studied are unity power factor control, and reaction control. The excitation current control methods are discussed thoroughly in paragraphs 3.3 and 3.4 respectively.

As it can be seen from Figure 2.2, several coordinate transformation blocks are used in the synchronous motor drive. To simplify control algorithms, low-level controllers input signals should be DC quantities, what can be reached by introducing several reference frames. For this reason, the following four control frames are introduced:

- rotor oriented control frame (dq-axes);
- stator oriented control frame (ψT-axes);
- orthogonal reference frame (αβ-axes);
- 3-phase reference frame (UVW-axes).

The control frames vector diagram is illustrated in Figure 2.3.

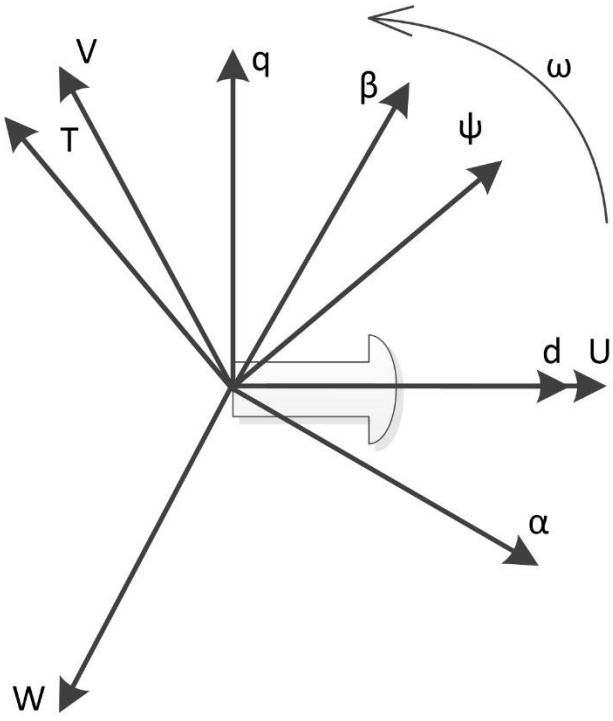

Figure 2.3 – Control and reference frames.

The rotor oriented reference frame, also referred to as the field oriented control frame as the rotor flux linkage is aligned with the d-axis (direct axis), and the q-axis (quadrature axis) is leading the d-axis by the angle of 90°. This reference frame allows the machine inductances not to be a function of rotor angle, preventing the inductance values change. Still, the inductances can be exposed to the saturation phenomena while the machine is operating in the field weakening range [1]. In the figure, the field oriented control frame is specified by dq-axes.

The idea behind the current control in the rotor reference frame, i.e. the field-oriented control, is to control the flux linkage and the torque independently by the regulation of the corresponding currents in d-axis ($\boldsymbol{i}_d$) and q-axis ($\boldsymbol{i}_q$). For this reason, the stator voltage equations decoupling schemes should be used to eliminate the dependence of the axis components on the other axes.

The field-oriented control frame is a rotational reference frame, what makes the controlled variables, i.e. the d- and q-axis stator currents, DC quantities; this fact allows to use simple PI controllers in the stator current low-level control.

The stator oriented reference frame is also referred to as the flux linkage control frame.

As its name suggests, this reference frame is used for the stator flux linkage control. The axes specifying the stator reference frame are the stator flux linkage $\boldsymbol{\psi}_s$, that aligns the flux producing current component $\boldsymbol{i}_\psi$, and the stator voltage $\boldsymbol{u}_s$, along that the torque producing current component $\boldsymbol{i}_T$. The axes are orthogonal to each other. The stator flux linkage and the electromagnetic torque are controlled by the corresponding current components. However, the reference frame transformation is required to obtain the current components references, as they are specified in the rotor oriented reference frame. Similar to the field oriented control frame, the flux linkage control frame is the rotational reference frame as well; the controlled variables are DC quantities as well.

The angle between the stator and rotor oriented reference frames is known as the load angle.

To perform the transformations from one reference frame to the other, the orthogonal reference frame is introduced. This reference frame is specified with the α-axes and β-axes with the 90° angle between them, and is the stationary reference frame.

The stator winding magnetic axes are referred to the 3-phase reference frame, specified by the U, V, W vectors located at 120° to each other. The stator reference frame is fixed in the U phase direction.

The reference frames usage and transformation between them can be described as follows. Firstly, the flux $\boldsymbol{i}_{\psi}$ and $\boldsymbol{i}_{T}$ torque producing current components are transformed from the stator oriented reference frame to the rotor oriented reference frame in accordance with the Park transformation technique; the current components $\boldsymbol{i}_{d}$ and $\boldsymbol{i}_{q}$ are now in the field oriented control frame. The current controller outputs are the voltage references in the rotor reference frame as well. To specify the reference phase values sent to the modulator bridge, the transformation to the 3-phase reference frame is required. This is implemented in two steps by applying the inverse Park and inverse Clarke transformation techniques. Current feedback signals also require the transformation from the 3-phase system to the dq-coordinates.

Park transformation is expressed by the following equations:

$$I_d = I_x cos\delta + I_y sin\delta \,, \tag{2.26}$$

$$I_q = I_y cos\delta - I_x sin\delta \,, \tag{2.27}$$

where δ is the load angle.

Inverse Park transformation is expressed by the following equations:

$$V_x = V_d cos\delta - V_q sin\delta \,, \tag{2.28}$$

$$V_y = V_q cos\delta + V_d sin\delta \,, \tag{2.29}$$

Inverse Clarke transformation is expressed by the following equations:

$$V_U = V_x \tag{2.30}$$

$$V_V = \frac{(-V_x + \sqrt{3}V_y)}{2} \tag{2.31}$$

$$V_W = \frac{\left(-V_x - \sqrt{3}V_y\right)}{2} \tag{2.32}$$

Coordinate transformation blocks are used in both direct path and feedback.

However, reference frame transformation techniques do not allow for separate control of quantities specified in different axes. For this purpose, a decoupling block is introduced. The decoupling block is used to eliminate cross-coupling-effects, i.e. the dependency of vectors

specified in different axes. Decoupling allows to tune stator current controllers in different axes separately and simultaneously.

The 'SVPWM' block represents space vector pulse width modulation, that is a contemporary PWM technique, providing advanced performance for variable frequency drive applications.

The voltage source inverter (VSI) represents the link between the power source and the drive motor. As the name implies, the DC line acts as a DC voltage source to the inverter. VSI provides the voltage output control in terms of both the frequency and the magnitude. The inverter output phase voltages are supplied to the EESM stator.

The blocks enclosed in the feedback represent the estimators. The stator flux linkage estimation is conducted based on the current model equations. Feedback signals are used to track the driven motor state, and generate control signals so that the error between these signals is eliminated. The main machine parameter in the feedback loop is the motor angular speed. In fact, the angular speed is estimated based on the rotor position. The driven motor phase voltages and excitation current are also measured and used as a feedback signals. As the phase voltages are in the 3-phase reference frame, inverse transformation to the rotor reference frame occurs.

Another crucial block inserted into the feedback is the flux limiter. The flux limiter allows to implement the EESM operation in the field weakening range.

The field weakening fundamental equation is reflected by the Faraday`s law:

$$\boldsymbol{u}_s \approx \boldsymbol{e}_s = \boldsymbol{\omega}_s \boldsymbol{\psi}_s \tag{2.33}$$

In accordance with the law, the stator voltage $\boldsymbol{u}_s$ rises proportionally to the angular speed $\boldsymbol{\omega}_s$ while the stator flux linkage $\boldsymbol{\psi}_s$ remains constant; $\boldsymbol{e}_s$ is the induced in the electric motor back emf. This statement is fair until the stator voltage is below the maximum available level. When the maximum available voltage value is reached (the feeding voltage), the subsequent speed increase is impossible without the stator flux linkage being reduced. To make the EESM operation possible at speeds higher than the nominal, the stator flux linkage is reduced by the value inversely proportional to the angular speed, what keeps the emf value lower than the stator voltage value [2]. The field starts weakening. The field weakening range is illustrated in Figure 2.4.

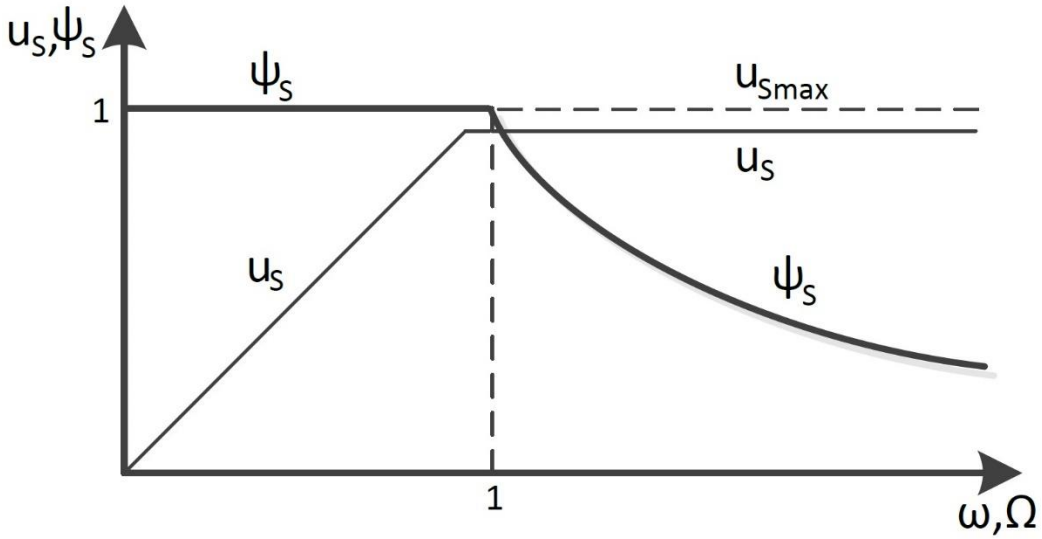

Figure 2.4 - Field weakening range.

As Figure 2.4 points out clearly, until the motor is operating in the speed range below the rated value (1 pu), the stator flux linkage remains constant at the level of 1 pu. As the speed exceeds the nominal value, the stator voltage remains constant at the level slightly less than maximum available voltage, while the stator flux linkage decreases in accordance with the equation (2.33).

The dynamic performance of the EESM drive in the field weakening range depends on the stator flux linkage and the excitation current. In accordance with equation (2.34), the field weakening motor operation also causes the electrical torque reduction.

$$\boldsymbol{T}_e = 1.5p(\boldsymbol{\psi}_d \boldsymbol{i}_q - \boldsymbol{\psi}_q \boldsymbol{i}_d) \tag{2.34}$$

In the field weakening range the voltage reserve should be maintained to ensure the stator voltage is not exceeded if sudden changes in torque occur. Generally, the voltage reserve is specified as 5%-10% of the voltage converter output [1]. In Figure 1.4 the voltage reserve is between the voltage levels u_{smax} and u_s.

The field weakening operation have the same principle for both DC and AC motors. However, electrical machines with external excitement allows for easier control in the field weakening range due to flux level regulation [1].

In accordance with the angular speed feedback values entering the flux limiter, the corresponding stator flux linkage values are supplied as a reference to the stator flux linkage controller. In fact, the flux limiter implements the diagram presented in Figure 2.4.

The working principle of the EESM functional scheme illustrated in Figure 2.1 can be explained as follows. Firstly, the phase ($\boldsymbol{i}_u$, $\boldsymbol{i}_v$, $\boldsymbol{i}_w$) and excitation ($\boldsymbol{i}_f$) currents are measured, the former being transformed to the rotor reference frame. The rotor angular speed $\boldsymbol{\omega}_r$ is measured as well. The measured currents are used to estimate the damper currents in dq-axes $\boldsymbol{i}_D$ and $\boldsymbol{i}_Q$ values, as well as the stator flux linkage actual value $\boldsymbol{\psi}_s$ in accordance with the machine currents mathematical model (2.21 – 2.25). Based on the flux linkage values, the load angle δ_s cosine and sine values are estimated, the values being transmitted to the reference frame transformation block to perform the transformation from the stator reference frame to the rotor frame. The angular speed value is measured not only to be transmitted to the speed controller, but also to the flux limiter block, where the stator flux linkage reference value corresponding to the actual rotor speed is selected. The stator currents in dq-axes are supplied to the corresponding controllers, the obtained at the controller's outputs voltages are decoupled, then converted to the orthogonal reference frame, and after the modulation in accordance with the SVPWM technique are transmitted to the VSI, where the inverted three-phase voltage is supplied to the EESM stator. The synchronous motor field winding is fed with the excitation voltage $\boldsymbol{u}_f$, obtained at the excitation controller output.

2.2 EESM drive model overview

The synchronous motor drive model is built in the MATLAB Simulink software in accordance with the drive structure presented and discussed in paragraph 2.1.

The model comprises two main parts: the electrically excited synchronous motor itself, and the control system; the power converter is simulated as well.

In this paragraph, the model and its components are described in detail.

The 'Control' block, that describes the control logic, is implemented as a subsystem. The subsystem combines the speed, flux, current components, and excitation low-level controllers. Each low-level controller is based on the PI-controller, that generates corrective actions if an error between reference and actual value exists. The 'Control' subsystem inputs are the speed reference, as well as the stator current, angular speed, and field (excitation) current feedback signals; the switching signals for the bridge, and the excitation voltage are the subsystem`s output signals.

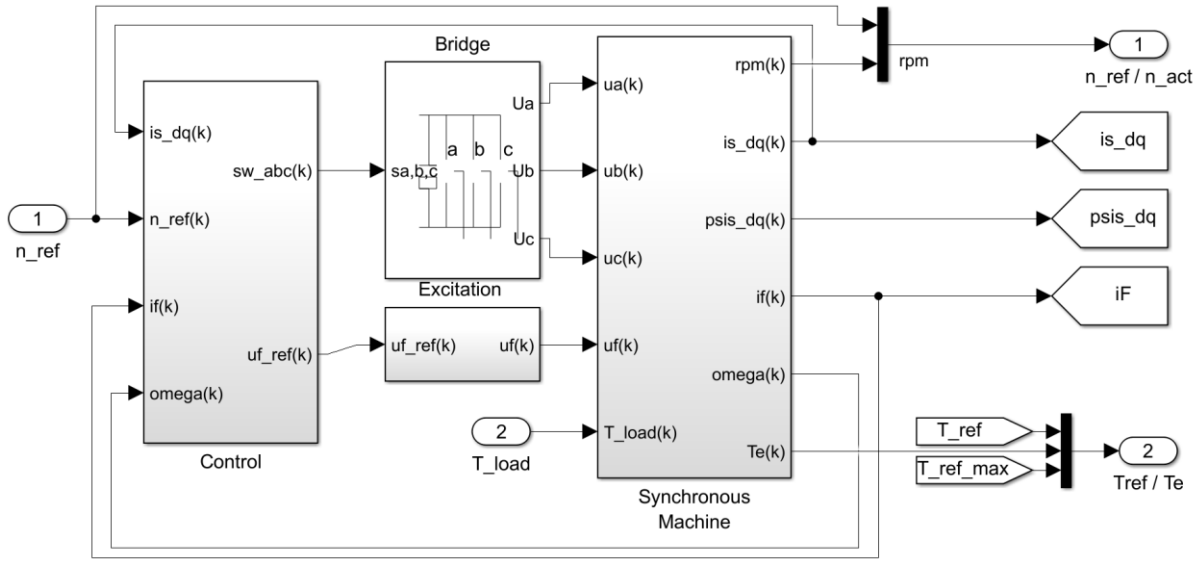

Figure 2.5 – EESM drive Simulink model.

The ‘Bridge’ block represents the voltage source inverter. The inverter receives signals generated by the control logic, and is switched in accordance with these signals; the output signal is the three-phase voltage.

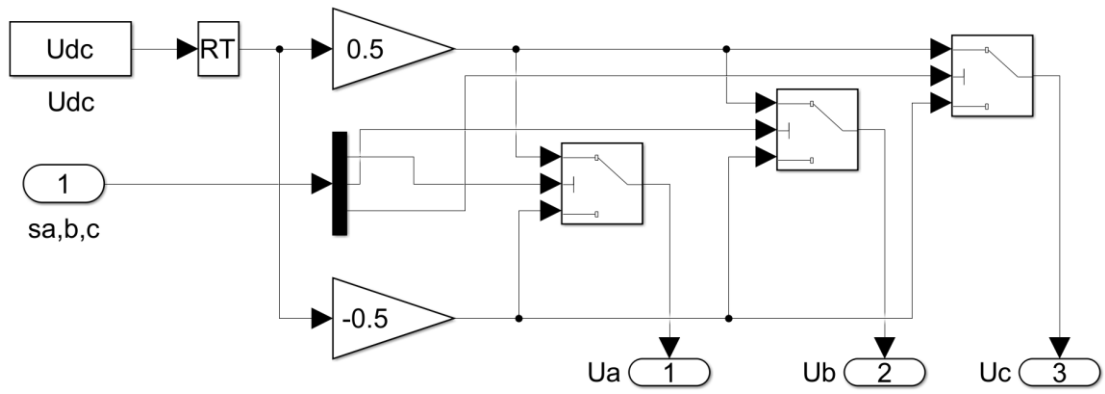

Figure 2.6 – Voltage source inverter model.

In the ‘Excitation’ block, the excitation voltage is transferred from the control logic to the synchronous motor electrical model. The presence of this block is essential in the scheme, because the Control and Synchronous Machine blocks operate at different rates. The synchronous motor model is a discrete one, and to avoid possible mistakes due to different sampling times in the main parts of the model, the rate transition block is required.

The ‘Synchronous Machine’ block is built to simulate the motor behavior and to make the synchronous motor drive research possible. The motor simulation model reflects the EESM

inner design, and contains electrical and mechanical parts. The electrical part is the voltage mathematical model equations (2.3 – 2.7) discretized within the modelling process.
The synchronous motor mechanical part is described with the equation:

$$\boldsymbol{\omega}_r = \int \frac{\boldsymbol{T}_e - \boldsymbol{T}_{load}}{J}, \tag{2.35}$$

Where $\boldsymbol{\omega}_r$ – rotor angular speed; $\boldsymbol{T}_e$ and $\boldsymbol{T}_{load}$ – electromagnetic and load torque respectively; J – inertia.
Each block in the whole model just refers to the actual synchronous motor parameters, as well as the reference vectors and values that are listed and calculated in a so-called mask inside the model. The motor parameters used in the model are listed in Table 2.1.
The reference vectors definition is presented in more detail in the following paragraphs.

Table 2.1 – Motor parameters

Parameter	*Value*
Apparent Power	14500 VA
Nominal voltage	400 V
Nominal current	21 A
Nominal field current	10.5 A
Nominal frequency	50 Hz
Nominal rotational speed	1500 rpm
Nominal power factor	0.8
Reduction factor	4.637
Pole pairs number	2
Motor inertia	0.1 kgm^2
Stator winding resistance	0.048 pu
Damper winding D-axis resistance R_D	0.02 pu
Damper winding Q-axis resistance R_Q	0.03 pu
Field winding resistance R_f	0.0083 pu
Stator winding stray inductance $L_{s\sigma}$	0.12 pu
Damper winding D-axis stray inductance $L_{D\sigma}$	0.07 pu
Damper winding Q-axis stray inductance $L_{Q\sigma}$	0.14 pu
Canay inductance $L_{k\sigma}$	0
Field winding stray inductance $L_{f\sigma}$	0.27 pu
Magnetizing inductance d-axis L_{md}	1.05 pu
Magnetizing inductance q-axis L_{mq}	0.45 pu

The EESM control system modification was started from the total discretization of the model, as the initial model, as well as its solver were time-continuous. For this reason, the

equations presented in paragraph 2.2 (2.3 – 2.7) were discretized using Tustin`s bilinear transformation in accordance with the formula:

$$s = \frac{2}{T_s}\,\frac{z-1}{z+1}, \tag{2.36}$$

where T_s – sampling time; the sampling time value used in the Simulink model equals 1 μs. The MATLAB Simulink solver used for the model simulation is 'Fixed Step Discrete'; the step size is equal to 1 μs.

The discretized voltage model of the EESM can be described with the equations:

$$\Delta\psi_d = \frac{T_s}{2}\left[\Delta u_d - R_s\left(\frac{C}{A}\Delta\psi_d - \frac{D}{A}\Delta\psi_D - \frac{E}{A}\Delta\psi_f\right) + \Delta\omega\Delta\psi_q\right] \tag{2.37}$$

$$\Delta\psi_q = \frac{T_s}{2}\left[\Delta u_q - R_s\left(-\frac{L_Q}{B}\Delta\psi_q - \frac{L_{mq}}{B}\Delta\psi_Q\right) - \Delta\omega\Delta\psi_d\right] \tag{2.38}$$

$$\Delta\psi_D = \frac{T_s}{2}\left[-R_D\left(\frac{F}{A}\Delta\psi_D - \frac{H}{A}\Delta\psi_f - \frac{D}{A}\Delta\psi_d\right)\right] \tag{2.39}$$

$$\Delta\psi_Q = \frac{T_s}{2}\left[-R_Q\left(\frac{L_q}{B}\Delta\psi_Q - \frac{L_{mq}}{B}\Delta\psi_q\right)\right] \tag{2.40}$$

$$\Delta\psi_f = \frac{T_s}{2}\left[\Delta u_f - R_f\left(\frac{G}{A}\Delta\psi_f - \frac{H}{A}\Delta\psi_D - \frac{G}{A}\Delta\psi_f\right)\right] \tag{2.41}$$

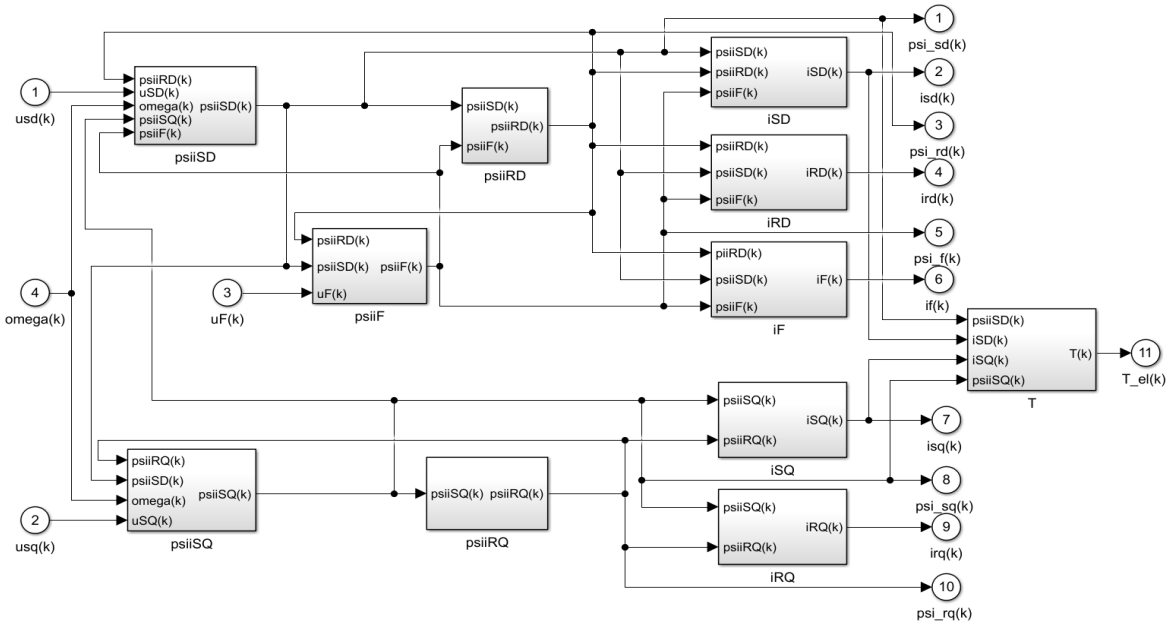

Figure 2.7 – Synchronous motor electrical model built in Simulink.

The synchronous motor model is implemented in Simulink in accordance with the discretized equations.

The stator voltages in d- and q-axes, the field winding (excitation) voltage, as well as the angular speed are the electrical model inputs; the only output is the electrical torque.

The motor inductances are modelled with no saturation assumed. However, as the inductances are functions of current flowing through it, these parameters are changed while testing the drive robustness.

In the next paragraph the controllers used in the EESM drive are discussed in more detail.

2.3 Controllers overview

In the EESM drive control system five low-level controllers are used: speed controller, stator flux controller, excitation controller, and stator current controller for both axes in the rotor reference frame.

The control algorithm studied does not allow for the separate control for the electromagnetic torque. As was mentioned before, the torque is controlled by the current component $\boldsymbol{i}_{\mathrm{T}}$, aligned with the stator voltage in the stator oriented control frame. The relation between the torque producing current component, and the torque and the stator flux linkage references is given by the equation:

$$\boldsymbol{i}_{Tref} = \frac{\boldsymbol{T}_{ref}}{1.5p\boldsymbol{\psi}_{sref}} \tag{2.42}$$

The speed control is achieved by adjusting the torque required at the set point. The input signals are actual and reference angular speed values. The reference speed is set as a repeating table, where the speed values are linked with the certain time instants. The angular speed actual value is obtained as a feedback signal. The error between these values is the PI-controller input, that generates the torque reference as output.

The stator flux linkage control is another important low-level control in the EESM drive. Both the stator and the excitation winding contribute to the stator flux control. As was shown in Figure 1.3, the stator flux linkage control is performed in the stator oriented control frame ψT-axes. The flux-producing current component $\boldsymbol{i}_{\psi}$ controls the flux, as well as the torque-producing current component $\boldsymbol{i}_{\mathrm{T}}$ is used to control the torque. These current components are

orthogonal to each other. However, as the current reference needed for the current control are in the field oriented control frame, the reference frame transformation is required. The control loop has stator flux linkage actual and reference values as inputs; the PI-controller output is the flux-producing current reference required. The stator flux linkage reference is obtained from the lookup table, that is physically the flux limiter. Depending on the speed reference, the corresponding flux linkage value is selected as a reference. The flux linkage limiter calculation is presented in paragraph 3.1. The actual stator flux linkage value is estimated in accordance with the current model (2.21 – 2.25). The EESM current model equations are presented in paragraph 2.2. The error between the reference and actual values are supplied to the PI-controller, that generates the flux producing current component reference value.

The excitation control also known as the field winding control is used to produce the machine flux, as well as contribute to the machine`s stability and performance. The equation describing the excitation current control is the following:

$$\boldsymbol{u}_f = R_f \boldsymbol{i}_f + \left(L_f - \frac{L_{fD}^2}{L_D} \right) \frac{d\boldsymbol{i}_f}{dt} - \frac{L_{fD} R_D}{L_D} \boldsymbol{i}_D \tag{2.43}$$

The inputs are the excitation (field winding) current and its reference, stator and rotor currents, while the only output is the excitation voltage. The field winding current reference is obtained by applying either the unity power factor principle or the reaction control technique, discussed in detail in paragraphs 3.3 and 3.4 respectively. The PI controller is fed with the error between the actual excitation current and its reference value. The controller output is then added to the difference between stator and rotor currents, that results in the excitation voltage.

The stator current control is used to form the current vectors of the length required in d- and q-axes. The input signals are the stator currents and its references in both axes, rotor currents, stator flux linkages, excitation current, and angular speed. The torque producing and flux producing current reference values are supplied to the reference frame transformation block, where the conversion from the orthogonal reference frame to the rotor reference frame occurs in accordance with Park transformation (2.26 – 2.27). The reference frame transformations are discussed thoroughly in paragraph 1.2. The errors between actual and

reference of the stator decoupled currents are supplied to the PI-controller. The current control loop outputs are the voltage references in d- and q-axes can be written as:

$$\boldsymbol{u}_{d,ref} = R_s \boldsymbol{i}_d + L_{cc,d} \frac{d\boldsymbol{i}_d}{dt} + \boldsymbol{e}_d \,, \tag{2.44}$$

$$\boldsymbol{u}_{q,ref} = R_s \boldsymbol{i}_q + L_{cc,q} \frac{d\boldsymbol{i}_q}{dt} + \boldsymbol{e}_q \,, \tag{2.45}$$

where $\boldsymbol{e}_d$ and $\boldsymbol{e}_q$ are the decoupling voltage terms expressed as follows:

$$\boldsymbol{e}_d = -\left(\boldsymbol{i}_D \frac{L_{md} R_D}{L_D}\right) + \left(L_{md} - \frac{L_{md}^2}{L_D}\right) \frac{d\boldsymbol{i}_f}{dt} - \boldsymbol{\psi}_q \boldsymbol{\omega} \tag{2.46}$$

$$\boldsymbol{e}_q = -\left(\boldsymbol{i}_Q \frac{L_{mq} R_Q}{L_Q}\right) + \boldsymbol{\psi}_d \boldsymbol{\omega} \tag{2.47}$$

The obtained reference voltages in d- and q-axes are then transformed firstly to the orthogonal reference frame, and after that to the stator reference frame in accordance with inverse Park (2.28 – 2.29) and inverse Clarke (2.30 – 2.32) transformation formulas respectively. The resulting voltages are transmitted through the modulator, that generates the control signals for the semiconductor bridge, i.e. voltage source inverter. The VSI is used to supply the controlled motor with the required phase voltages.

The stator current controllers tuning process is discussed in more detail in paragraph 3.2.

2.4 Torque limiter

In order to enhance the drive performance, the reference torque limiter is introduced. The limiter is implemented as a dynamic saturation block, that has three inputs: the controlled signal, that is torque reference; the upper limit, that is presented by the maximum torque reference; the lower limit, that is specified as the maximum torque reference with the minus sign. In fact, it is not the torque reference that should be limited, but the load angle, that is directly proportional to the torque. In accordance with equation (2.34), the torque reference limitation reduces the load angle as well, preventing the synchronism loss possibility. Moreover, the dynamic saturation block used after the speed PI controller allows to prevent

the integration wind-up situation. The whole controller structure implemented in the Simulink model is illustrated in Figure 2.8.

The controller gains are specified as discussed in paragraph 3.2. The back-calculation coefficient Kb is equal to 1. As it can be seen from the block diagram, the controller output is subtracted from the saturation block output; the error is summed with the feedback before the following integration.

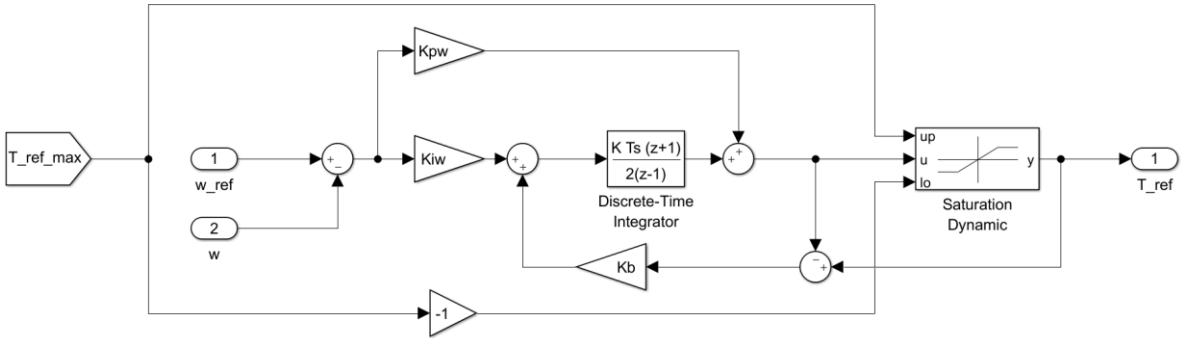

Figure 2.8 – Speed controller model.

As a chapter conclusion, the EESM drive model was discussed in detail. Electrically excited synchronous motor voltage and current models, the power converter, and the control frames used were presented, the field weakening technique and torque limiter were introduced, and the low-level control loops were discussed. In the next chapter the tuning process of the EESM drive is described.

3. DYNAMIC PERFORMANCE AND ROBUSTNESS ANALYSIS

In the previous chapter the synchronous motor drive model built in MATLAB Simulink was introduced. However, to achieve high dynamic performance in field weakening, the control system should be tuned properly. For this reason, the model adjustments required are proposed and explained, and the EESM tuning process is discussed thoroughly.

The drive tuning parameters studied in the current work are as follows:

- stator flux linkage reference vector;
- stator current controller parameters;
- load torque rise time;
- excitation control method.

The control system design discussed above and the model built in Simulink are based on the ideal case assumption. However, to ensure the control system robustness, the worst-case scenario should be analyzed as well. For this reason, during the drive analysis the parameters uncertainty should be considered. Robustness is an ability of a control system to keep insensitivity to disturbances and parameters fluctuations [3]. A trade-off between the drive robustness and its performance is an important issue to consider while designing a control system.

Finally, the resulting model versions are listed to be tested and simulated in terms of dynamic performance and robustness in the following chapter.

3.1 Stator flux linkage reference definition

In this paragraph, the impact of the stator flux linkage reference on the drive performance in the field weakening range is discussed.

In the EESM drive the stator flux linkage reference is used in the flux low-level control, where the error between the actual and reference flux linkage values is supplied to the PI-controller, that has a flux producing current component $\boldsymbol{i}_{\psi}$ as an output. Besides that, based on the stator flux linkage reference the excitation current reference is calculated in accordance with either the unity power factor principle or the reaction control technique, discussed in paragraphs 3.3 and 3.4 respectively. The maximum torque reference calculation formula has the stator flux linkage reference as a factor as well:

$$\boldsymbol{T}_{ref\ max} = \frac{1.5p\boldsymbol{\psi}_{ref}\boldsymbol{\psi}_{md}}{L_{s\varsigma}} \tag{3.1}$$

The torque producing current reference $\boldsymbol{i}_{Tref}$ calculation is given by the equation (2.49).

As it can be seen from the equations, the stator flux linkage reference vector definition is a crucial design step, as it affects directly the excitation current reference value and torque produced.

The stator flux linkage reference value for a certain operational point is calculated following the sequence in an iterative cycle:

$$\delta = \operatorname{atan}\left(\frac{L_q T_e}{\boldsymbol{\psi}_s^2}\right), \tag{3.2}$$

$$\boldsymbol{i}_d = -\frac{\boldsymbol{T}_e}{\boldsymbol{\psi}_s}\sin(\delta)\,, \tag{3.3}$$

$$\boldsymbol{i}_q = \frac{\boldsymbol{T}_e}{\boldsymbol{\psi}_s}\cos(\delta), \tag{3.4}$$

$$\boldsymbol{i}_f = \frac{\left(\boldsymbol{\psi}_s^2 + L_d\frac{\boldsymbol{T}_e}{\boldsymbol{\psi}_s^2}\right)}{L_{md}\sqrt{\boldsymbol{\psi}_s^2 + L_q^2\left(\frac{\boldsymbol{T}_e}{\boldsymbol{\psi}_s}\right)^2}}, \tag{3.5}$$

$$\boldsymbol{\psi}_d = L_d\boldsymbol{i}_d + L_{md}\boldsymbol{i}_f\,, \tag{3.6}$$

$$\boldsymbol{\psi}_q = L_q\boldsymbol{i}_q\,, \tag{3.7}$$

$$\boldsymbol{\psi}_s = \sqrt{\boldsymbol{\psi}_d^2 + \boldsymbol{\psi}_q^2}\,, \tag{3.8}$$

$$\boldsymbol{u}_d = R_s\boldsymbol{i}_d - \boldsymbol{\omega}\boldsymbol{\psi}_q\,, \tag{3.9}$$

$$\boldsymbol{u}_q = R_s\boldsymbol{i}_q + \boldsymbol{\omega}\boldsymbol{\psi}_d\,, \tag{3.10}$$

$$\boldsymbol{u}_s = \sqrt{\boldsymbol{u}_d^2 + \boldsymbol{u}_q^2} \tag{3.11}$$

Firstly, the flux linkage initial value is specified; the operational point, i.e. the torque load and angular speed per unit values are specified as well. In accordance with the equations (3.2 – 3.11), the stator flux linkage and voltage are calculated, and if the stator voltage exceeds the unity, the stator flux linkage reference value should be reduced.

The calculation example for the operational point of double nominal speed under 150% load is presented further.

$$\delta = \operatorname{atan}\left(\frac{0.57 * 1.5}{(0.413)^2}\right) = 1.3739$$

$$\boldsymbol{i}_d = -\frac{1.5}{0.413}\sin(1.3739) = -3.5618$$

$$\boldsymbol{i}_q = \frac{1.5}{0.413}\cos(1.3739) = 0.7106$$

$$\boldsymbol{\psi}_d = 1.17 * (-3.5618) + 1.05 * 4.0458 = 0.0808\,,$$

$$\boldsymbol{\psi}_q = 0.57 * 0.7106 = 0.405$$

$$\boldsymbol{\psi}_s = \sqrt{0.0808^2 + 0.405^2} = 0.413$$

$$\boldsymbol{u}_d = 0.048 * (-3.5618) - 2 * 0.405 = -0.981$$

$$\boldsymbol{u}_q = 0.048 * 0.7106 + 2 * 0.0808 = 0.1957$$

$$\boldsymbol{u}_s = \sqrt{(-0.981)^2 + 0.1957^2} = 1.0003$$

The stator flux linkage reference for speed values in the range of 0 – 4125 rpm are presented in Table 3.1.

Table 3.1 – Calculated stator flux linkage reference values

Stator flux linkage reference values, pu										
1.0	1.0	1.0	1.0	0.720	0.583	0.486	0.413	0.353	0.306	0.265
Speed values, rpm										
0	500	1000	1500	1875	2250	2625	3000	3375	3750	4125

As it can be seen from Table 3.1, the stator flux linkage reference vector is, in fact, a flux limiter, mentioned in paragraph 2.2. Until the speed value is kept below the nominal speed, that equals 1500 rpm, the stator flux linkage reference value is kept at unity. At speeds exceeding the nominal value a smooth reduction of flux linkage is implemented, the reference value for double nominal speed being half of the nominal stator flux linkage. Thus, the field weakening main condition is realized in the model. In the model the values calculated for the stator flux linkage reference are stored inside the lookup table block. The output signal from the stator flux linkage lookup table is supplied to the flux controller and to the excitation current calculation block.

3.2 Stator current control tuning

Another important issue to consider is the stator current rise time, that is the stator current control tuning parameter.

In the stator current control loop a PI-controller is used. One of the most efficient ways to tune the controller gains is the Internal Model Control method [4]. In accordance with IMC, the PI-controller parameters can be specified based on certain machine parameters, and required system performance specifications, i.e. the rise time and bandwidth. Another benefit of this tuning method is the cross coupling between d- and q- axis elimination, what allows to tune two controllers in the d- and q-axis loops simultaneously.

The PI-controller proportional and integral gains (K_p and K_i respectively) can be determined by selecting the desired bandwidth in accordance with the formulas [1]:

$$K_p = \alpha_{cc} L_{cc,dq}\,, \tag{3.12}$$

$$K_i = \frac{L_{cc,dq}}{R_s}\,, \tag{3.13}$$

where α_{cc} is the specified closed loop bandwidth; R_s – stator winding resistance. The current control inductances in d- and q-axis $L_{cc,dq}$ can be written as:

$$L_{cc,d} = L_d - \frac{L_{md}^2}{L_D}\,, \tag{3.14}$$

$$L_{cc,q} = L_q - \frac{L_{mq}^2}{L_Q}\,, \tag{3.15}$$

where L_d and L_q are stator inductances in d- and q-axis respectively; L_D and L_Q – rotor inductances in d- and q-axis respectively; L_{md} and L_{mq} – magnetizing inductance in d- and q-axis respectively.

Instead of specifying the desired bandwidth value, the current control rise time can be chosen instead; the relation between these values is given by the formula:

$$\alpha = \frac{ln\,9}{t_r} \tag{3.16}$$

The stator current PI-controller gains for the rise time equaling 5ms are the following:

$$\alpha_{cc} = \frac{ln\,9}{t_{r,cc}} = 439.445$$

$$K_{pd} = \alpha_{cc}(L_d - \frac{L_{md}^2}{L_D}) = 81.572$$

$$K_{id} = \frac{L_{cc,d}}{R_s} = 3.864$$

$$K_{pq} = \alpha(L_q - \frac{L_{mq}^2}{L_Q}) = 99.657$$

$$K_{iq} = \frac{L_{cc,q}}{R_s} = 4.724$$

The excitation current control has the same tuning principles as the stator current control. The PI-controller gains can be determined by selecting the desired bandwidth in accordance with the equations [1]:

$$\alpha_f = \frac{ln\,9}{t_{r,f}} \tag{3.17}$$

$$K_{pf} = \alpha_f \left(L_f - \frac{L_{fD}^2}{L_D}\right) \tag{3.18}$$

$$K_{if} = \alpha_f R_f \tag{3.19}$$

The excitation current PI-controller gains for the rise time equaling 5 ms are the following:

$$\alpha_f = \frac{ln\,9}{t_{r,f}} = 439.445$$

$$K_{pf} = \alpha_f(L_f - \frac{L_{fD}^2}{L_D}) = 147.489$$

$$K_{if} = \frac{L_{cc,d}}{R_s} = 3.647$$

By specifying the desired stator and excitation currents rise time values, different controller gains can be obtained, that affects the drive dynamic performance.

3.3 Unity power factor excitation control

The unity power factor excitation control is the execution method of the excitation current reference calculation. The excitation current, also known as the field winding current, is an important design variable. In accordance with the unity power factor control principle, the excitation current reference can be expressed in the following form:

$$\boldsymbol{i}_{f\,ref} = \frac{L_d L_q \left(\frac{\boldsymbol{T}_{ref}}{\frac{3}{2} p \boldsymbol{\psi}_{ref}} \right)^2 + \boldsymbol{\psi}_{ref}^2}{L_{md} \sqrt{L_q^2 \left(\frac{\boldsymbol{T}_{ref}}{\frac{3}{2} p \boldsymbol{\psi}_{ref}} \right)^2 + \boldsymbol{\psi}_{ref}^2}} \tag{3.20}$$

The load angle equation at the unity power factor is the following:

$$\delta_s = \operatorname{atan}\left(\frac{\boldsymbol{T}_e L_q}{\boldsymbol{\psi}_s^2} \right) \tag{3.21}$$

In the model to calculate the load angle the estimated torque is used; the torque is calculated in accordance with the equation:

$$\boldsymbol{T}_e = \frac{3}{2} p (\boldsymbol{\psi}_{sd} \boldsymbol{i}_{sq} - \boldsymbol{\psi}_{sq} \boldsymbol{i}_{sd}) \tag{3.22}$$

Equation (3.22) is reflected in the model as a subsystem calculating the excitation current reference before it is applied to the excitation controller. The field current calculation subsystem is presented in Figure 3.1.

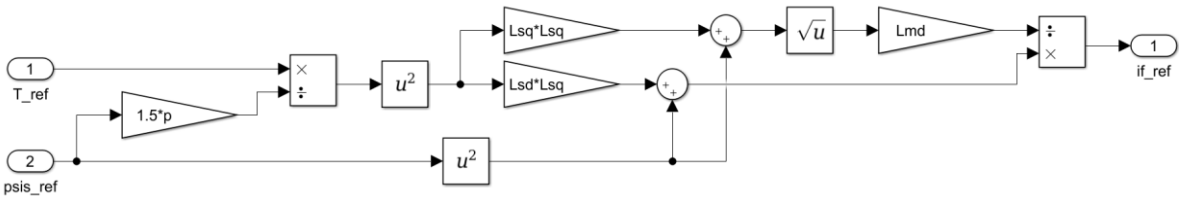

Figure 3.1 – Excitation current calculation.

As it can be seen from both the equation (3.22) and the model (Figure 3.1), the excitation current reference is the function of the stator flux linkage reference value and the torque reference. The stator flux reference adjustment is described in paragraph 3.1.
The further enhancement of the drive model dynamic performance can be obtained by tuning the load torque rise time. Even though the rise time increase slows down the dynamic performance, the transient might be enhanced by slight increase made in the load rise time.

3.4 Reaction excitation control

Another way of adjusting the drive performance in the field weakening range is the reaction excitation control technique. In the reaction control method introduced by Mård in 1990 the air gap flux linkage d-axis component $\boldsymbol{\psi}_{md}$ is kept constant, what allows to compensate the damper winding current in the d-axis $\boldsymbol{i}_D$ [1][2]. The fundamental equation of the reaction control reflects the Lenz`s law:

$$\Delta \boldsymbol{i}_f = -\Delta \boldsymbol{i}_d \tag{3.23}$$

The excitation current $\boldsymbol{i}_f$ compensates the stator current maintaining the stator power factor required. The excitation current reference $\boldsymbol{i}_{f\,ref}$ can be calculated in accordance with the equation:

$$\boldsymbol{i}_{f\,ref} = \frac{1}{L_{md}}\left[\left(\boldsymbol{\psi}_{ref} - L_d \boldsymbol{i}_{\psi}\right)\cos(\delta_s) + L_d \frac{\boldsymbol{T}_{ref}}{\frac{3}{2} p \boldsymbol{\psi}_{ref}} sin(\delta_s)\right], \tag{3.24}$$

where

$$\boldsymbol{i}_{T,ref} = \frac{\boldsymbol{T}_{ref}}{\frac{3}{2}p\boldsymbol{\psi}_{ref}} \tag{3.25}$$

The equation for the load angle δ_s at the changing power factor is given by the formula:

$$\delta_s = \operatorname{atan}\left(\frac{\boldsymbol{T}_e L_q}{\frac{3}{2}p\left(\boldsymbol{\psi}_s^2 - L_q\boldsymbol{\psi}_s\boldsymbol{i}_\psi\right)}\right) \tag{3.26}$$

The relation between flux- and torque producing current components ($\boldsymbol{i}_\psi$ and $\boldsymbol{i}_T$ respectively) is given by the formula:

$$\boldsymbol{i}_\psi = \boldsymbol{i}_T \tan(\phi)\,, \tag{3.27}$$

where ϕ is the function of the power factor:

$$\phi = \operatorname{acos}(PF) \tag{3.28}$$

In the model, the flux producing current component $\boldsymbol{i}_\psi$ should be set artificially, the value being selected based on the power factor required. Thus, the $\boldsymbol{i}_\psi$ can be specified assuming different power factor values (PF) in accordance with the equation:

$$\boldsymbol{i}_\psi = \boldsymbol{i}_T \tan\big(\operatorname{acos}(PF)\big)\,, \tag{3.29}$$

or avoiding trigonometric functions:

$$\boldsymbol{i}_\psi = \boldsymbol{i}_T \frac{\sqrt{1 - PF^2}}{PF} \tag{3.30}$$

In the model the power factor value is specified in the following way.

The power factor is a function of torque, and the dependence between these variables is approximated to be linear. As the load torque increases from zero value to the specified working point (1.5 pu), the corresponding change in the power factor value occurs.

In the model the dependence between these variables is implemented as a lookup table. The power factor working point value is equal to unity; to determine the initial excitation current value the following equations should be solved [2].

The steady state excitation current can be calculated in accordance with the formula:

$$\boldsymbol{i}_{f\,ref} = \frac{|\boldsymbol{\psi}_s|^2_{ref} + L_{sd}L_{sq}\dfrac{|\boldsymbol{T}_e|^2_{ref}}{|\boldsymbol{\psi}_s|^2_{ref}}}{L_{md}\sqrt{|\boldsymbol{\psi}_s|^2_{ref} + L^2_{sq}\dfrac{|\boldsymbol{T}_e|^2_{ref}}{|\boldsymbol{\psi}_s|^2_{ref}}}} \tag{3.31}$$

The load angle equation is given by the formula:

$$\delta = \operatorname{atan}\left(\frac{|\boldsymbol{T}_e|_{ref}L_{sq}}{|\boldsymbol{\psi}_s|^2_{ref}}\right) \tag{3.32}$$

The d-axis stator flux linkage component can be obtained by solving the equation:

$$\boldsymbol{\psi}_{sd} = \frac{1}{\sqrt{tan^2\delta + 1}}|\boldsymbol{\psi}_s|_{ref} \tag{3.33}$$

The d-axis current component can be calculated as follows:

$$\boldsymbol{i}_d = \frac{\boldsymbol{\psi}_{sd}}{L_{sd}} - \frac{L_{md}}{L_{sd}}\boldsymbol{i}_f \tag{3.34}$$

The initial excitation current value can be calculated according to the equation:

$$i_{f0} = \frac{L_{sd}(i_f + i_d) - \psi_{d0}}{L_{sd} - L_{md}} \tag{3.35}$$

The value calculated for the initial excitation current i_{f0} is equal to 2.23.

The Simulink drive model subsystem representing the excitation current reference calculation using the reaction control technique in accordance with equations (3.31 – 3.33) is shown in Figure 3.2.

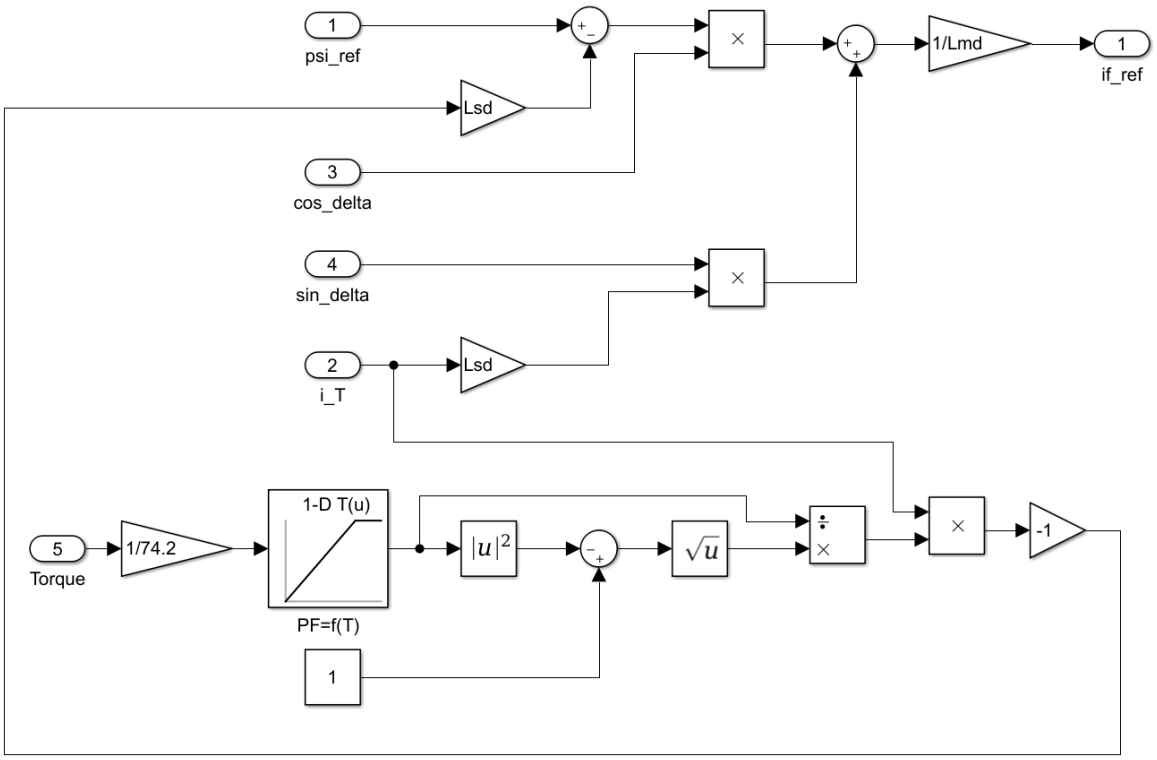

Figure 3.2 – Reaction control implementation.

The input parameters of the subsystem calculating the reference are the stator flux linkage and the torque references obtained during the previous control steps, as well as the current components and the load angle sine and cosine values.

In the model the reaction excitation control technique is switched on after the speed of double nominal value is reached. During the motor acceleration process, the excitation current reference is calculated in accordance with the unity power factor principle. When the level of double nominal speed is reached, the minor load (5%) is applied to overexcite the motor; until the total load torque is applied, the drive operates in the partial load mode. At the moment of torque load application the power factor starts to change its value in accordance with the lookup table, reaching the unity in the steady state. The initial power factor value, corresponding to the 5% load torque, is equal to 0.152. The final working point is the 150% load torque. The transitional values are formed by the linear approximation between the initial and final working points.

3.5 Robustness analysis

Robustness is a system stability quality to keep low sensitivity and good disturbance rejection [3]. The FOC EESM drive robustness is an important subject for consideration, since the inductances values are assumed being constant and accurate enough to match the hardware parameters. This assumption is not always valid, as the motor inductances can be subject to saturation, especially in the field weakening range. The saturation phenomena might pose a threat to the torque and the air-gap flux produced; the robustness analysis is required to predict the drive behavior if the saturation in the inductances occurs.

To conduct the robustness analysis, 10% change in the machine magnetizing inductance parameters is assumed. The parameters supposed to be changed are the d- and q-axis magnetizing inductances L_{md} and L_{mq}; due to the saturation, these values are reduced by 10%. However, as the model was built in such a way that the controllers are tuned based on the inductances specified in the mask, the parameters change should be implemented directly in the synchronous motor electrical part subsystem.

To improve the control system robustness, a new estimator is introduced. The flux linkage estimator, originally based on the machine current model, is transformed into the voltage model based estimator with the current model based correction term [19]. The correction term is calculated by the controller that has the error between the stator flux linkages obtained from the current model and voltage model as an input; the correction value is subtracted from the flux linkages calculated in accordance with the voltage model. Such a topology brings a certain benefit: the current model based estimator is more efficient at lower speeds (not exceeding the nominal value), while the voltage model is mostly suitable for operation at higher speeds. However, the voltage model based flux linkage estimator cannot be used directly: the machine state at the starting point does not allow for precise estimation of the stator flux linkages. As a controlling device, PI controllers are used for d- and q-axis. The voltage model based estimator is more beneficial in terms of robustness in comparison with the current model based estimator, as the equations does not contain inductances values. Thus, in the situation when the magnetizing inductances parameters are assumed to be a subject for saturation, and therefore wrong, the flux linkage estimator does not lose its precision.

The stator flux linkages in dq-axes calculated in accordance with the current model can be written as:

$$\boldsymbol{\psi}_d = \frac{L_{md}}{L_D}\boldsymbol{\psi}_D + \frac{L_d L_D - L_{md}^2}{L_D}\boldsymbol{i}_d + \frac{L_{md}L_D - L_{md}^2}{L_D}\boldsymbol{i}_f\,, \tag{3.36}$$

$$\boldsymbol{\psi}_q = \frac{L_{mq}}{L_Q}\boldsymbol{\psi}_Q + \frac{L_q L_Q - L_{mq}^2}{L_Q}\boldsymbol{i}_q\,, \tag{3.37}$$

where the damper winding flux linkages are:

$$\boldsymbol{\psi}_D = \frac{L_{md}}{1 + T_D s}(\boldsymbol{i}_d + \boldsymbol{i}_f)\,, \tag{3.38}$$

$$\boldsymbol{\psi}_Q = \frac{L_{mq}}{1 + T_Q s}\boldsymbol{i}_q\,, \tag{3.39}$$

where

$$T_D = \frac{L_D}{R_D}\,,\; T_Q = \frac{L_Q}{R_Q} \tag{3.40}$$

The stator flux linkages in dq-axes calculated in accordance with the voltage model can be written as:

$$\frac{d}{dt}\boldsymbol{\psi}_d = \boldsymbol{u}_d - R_s\boldsymbol{i}_d + \boldsymbol{\omega}\boldsymbol{\psi}_q - u_{comp,d}\,, \tag{3.41}$$

$$\frac{d}{dt}\boldsymbol{\psi}_q = \boldsymbol{u}_q - R_s\boldsymbol{i}_q + \boldsymbol{\omega}\boldsymbol{\psi}_d - u_{comp,q}\,, \tag{3.42}$$

where the compensated voltage $u_{comp,dq}$ generated by the PI controllers can be found as a difference between the fluxes obtained from the voltage and current models:

$$u_{comp,d} = K_p\left(\boldsymbol{\psi}_d^v - \boldsymbol{\psi}_d^i\right) + \frac{K_p}{T_I}\int\left(\boldsymbol{\psi}_d^v - \boldsymbol{\psi}_d^i\right)\,, \tag{3.43}$$

$$u_{comp,q} = K_p\left(\boldsymbol{\psi}_q^v - \boldsymbol{\psi}_q^i\right) + \frac{K_p}{T_I}\int\left(\boldsymbol{\psi}_q^v - \boldsymbol{\psi}_q^i\right) \tag{3.44}$$

To calculate the damper winding currents the following equations are used:

$$\boldsymbol{\psi}_D = \frac{L_D}{L_{md}}\boldsymbol{\psi}_d - \frac{L_d L_D - L_{md}^2}{L_{md}}\boldsymbol{i}_d - \frac{L_{md}L_D - L_{md}^2}{L_{md}}\boldsymbol{i}_f\,, \tag{3.45}$$

$$\boldsymbol{\psi}_Q = \frac{L_Q}{L_{mq}}\boldsymbol{\psi}_q - \frac{L_q L_Q - L_{mq}^2}{L_{mq}}\boldsymbol{i}_q \tag{3.46}$$

The estimator Simulink model built in accordance with the equations (3.36 – 3.46) is illustrated in Figure 3.3.

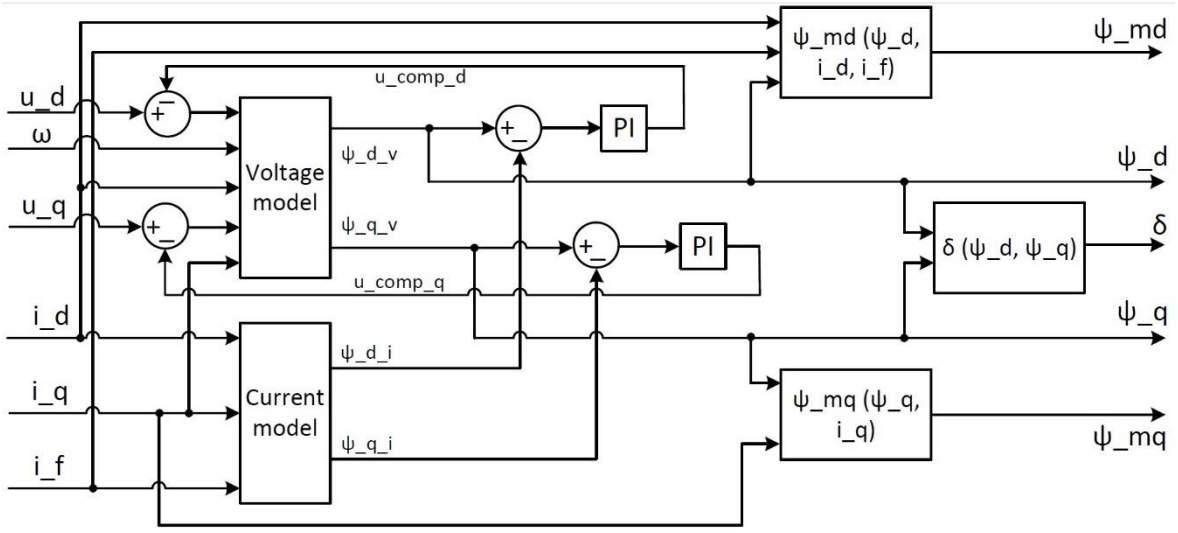

Figure 3.3 – The voltage and current models based flux linkage estimator model built in Simulink.

As it can be seen from the block diagram, the estimator inputs are the stator currents and voltages in dq-axes, the excitation current, and the rotor angular speed.

In this chapter the EESM drive model tuning parameters and possible dynamic performance improvements were discussed and the calculations required were made. In the next chapter the proposed tuning combinations are simulated and compared with theoretically assumed results and between each other; the robustness is analyzed as well.
The next stage of the EESM drive research is the proposed models simulations in MATLAB Simulink discussed in the next chapter.

4. SIMULATION RESULTS

In the current chapter the simulation results of the model with the tuned parameters as described in chapters 2, 3 are presented and analyzed.

The results obtained during the simulations are compared in order to determine how the tuning techniques discussed previously affects the drive performance, and what is the most efficient tuning combination among the simulated.

The importance of this control system development stage cannot be overestimated. The drive dynamic performance is studied in the MATLAB Simulink software by analyzing the torque and speed steps, what allows to prevent various time-consuming and high-cost errors occurrence while conducting the hardware tests. The torque transients measure is the settling time (in the current research, 1% error band is used), and the overshoot; the speed transient is analyzed by the speed drop due to the load application, as well as the settling time (since the velocity accuracy is required to be high, 0.1% error band is used). In accordance with the F. Franklin`s book, the settling time is the time of the system`s transient decay; the overshoot is the ratio between the maximum amount the system exceeds its final value, and the final working point [3].

To analyze the operation behavior during transients, steady-state, and field weakening, several experiments are conducted. The robustness test is carried out as well to analyze the drive`s ability to withstand the magnetizing inductances saturation. As the result, the tuning combination providing the highest dynamic performance level among the simulated tests was selected.

In the model the tuning parameters default values are specified. The speed ramp rise time from zero to double nominal speed (3000 rpm) is equal to 1.425 seconds; this time choice ensures the drive stability, and its accordance with the laboratory equipment simulated in the model. At the time instant of 1.625 seconds the minor torque load specified as 5% of nominal torque value is applied; the full torque of 150% is loaded at 2.2 seconds. The torque load rise time default value is specified as 20 milliseconds; the stator and excitation currents rise time are equal to 5 milliseconds. The stator flux linkage reference vector is determined primarily, since this vector strongly affects the drive performance; the correctness of the reference vector calculation described in paragraph 3.1 is checked during the first test, and the resulting reference values are used at all the following tests.

The model is simulated for 3.5 seconds; the first 1.425 seconds the electrical motor reaches double nominal speed; the time instant of 1.625 s – 2.2 s is the steady state region, the machine works at double nominal speed with a partial load; at 2.5 seconds the torque load is applied, and until 3.5 seconds the motor is trying to get back to steady state.

4.1 Unity power factor excitation control simulation

In this paragraph the simulation results of the control system, working at the unity power factor principle are presented.
Three experiments are conducted: in the first one the definition correctness of the stator flux linkage reference vector; in the second simulation, the rise time of the torque load is tested; in the third test the stator current rise time impact on the drive dynamic performance is studied.

Stator flux linkage reference vector definition

In this subparagraph, the definition correctness of the stator flux linkage reference vector is investigated. The stator flux reference values are specified as discussed in paragraph 3.1 (Table 3.1). The other tuning parameters default values remain.
The EESM drive operational process simulated in the full range is presented in Figure 4.1.

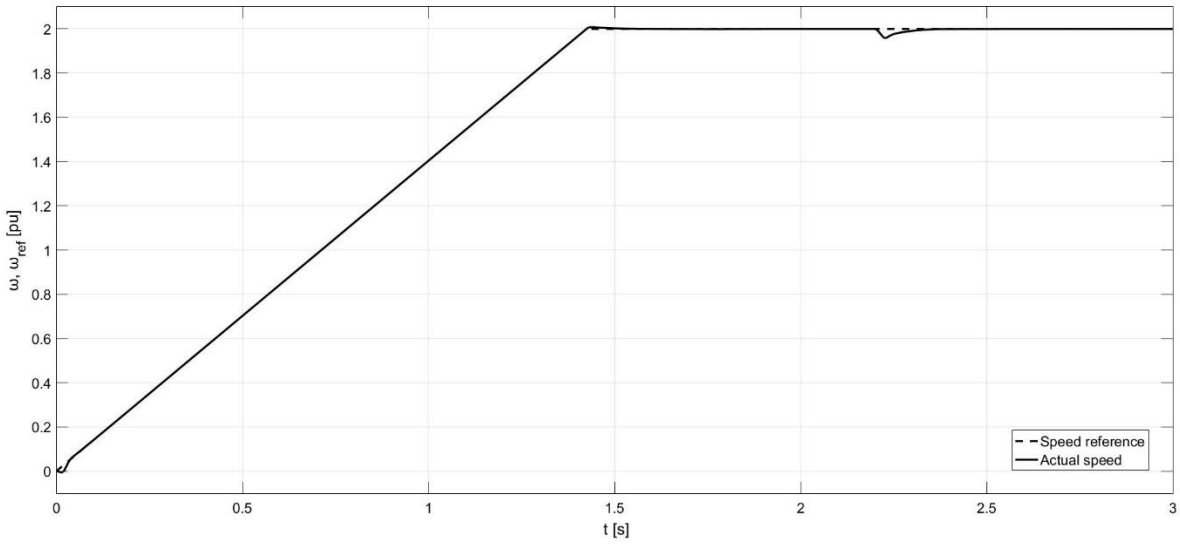

Figure 4.1 – Speed transient. The stator flux linkage reference vector is specified as presented in Table 3.1; the other tuning parameters remain the default values. The actual rotor speed

coincides with the reference speed. The speed drop seen between the time instants of 2.2 and 2.4 is due to the torque load application.

As it is illustrated in Figure 4.1, firstly, the motor starts its acceleration to the speed level of 2 pu, i.e. 3000 rpm. The acceleration process lasts for 1.425 seconds; since the time instant of 0.7 seconds the motor operates in the field weakening range. Until the time instant of 2.2 seconds the machine works in steady state at the speed level reached; then, the torque load of 1.5 pu, i.e. 111.3 Nm, is applied. At that point, the synchronous motor works under the load.
The motor actual speed follows the reference value precisely, with a minor deviation starting from the load torque application moment that lasts for 0.2 seconds. The corresponding torque transient is shown in Figure 4.2.

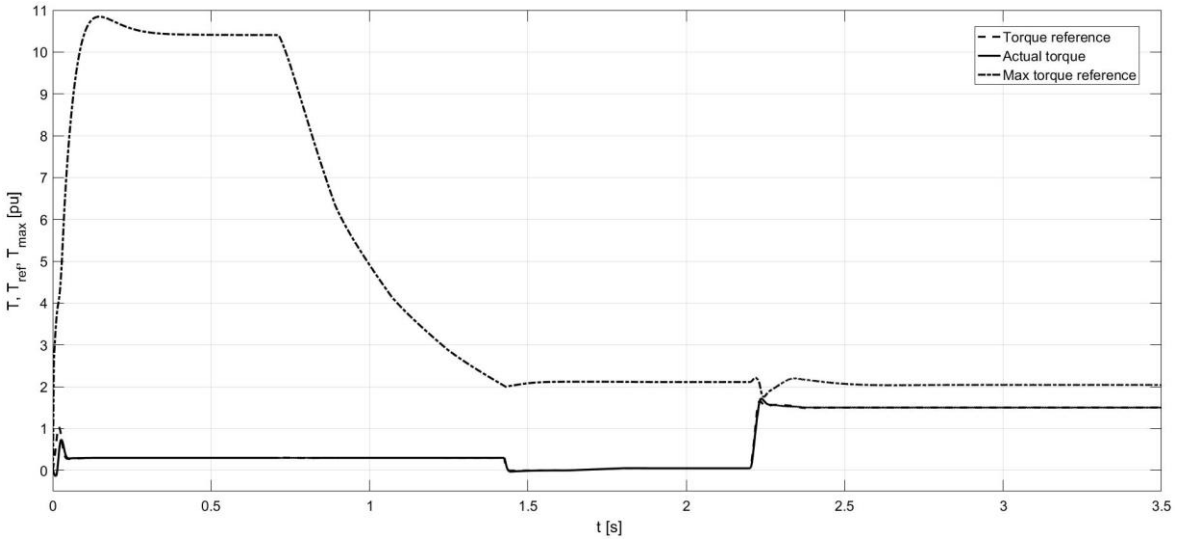

Figure 4.2 – Torque transient. The stator flux linkage reference vector is specified as presented in Table 3.1; the other tuning parameters remain the default values. The actual torque follows the reference torque precisely for the full operational range. The maximum torque reference reflects the torque level that the machine can provide not exceeding the 90° load angle, and thus, preventing it from the synchronism loss.

Illustrated in Figure 4.2 the torque curves correspond to the speed transient shown in Figure 4.1. During the time of the motor acceleration to the double nominal speed, the reference and actual torque is kept at a constant level. Then, the torque has almost zero level, gradually increasing to the level of 0.05, i.e. to 5% minor torque load, required to the reaction

excitation control principle. At the time instant of 2.2 seconds 150% load torque, i.e. 1.5 in per unit value, is applied. In the first simulation, the load torque rise time is specified as 20 ms, and since the torque is settled, the machine works under the load in the field weakening range.

To determine the settling time, and the overshoot, the extended fragments of the torque and speed steps after the torque load application are presented in Figures 4.3 – 4.4.

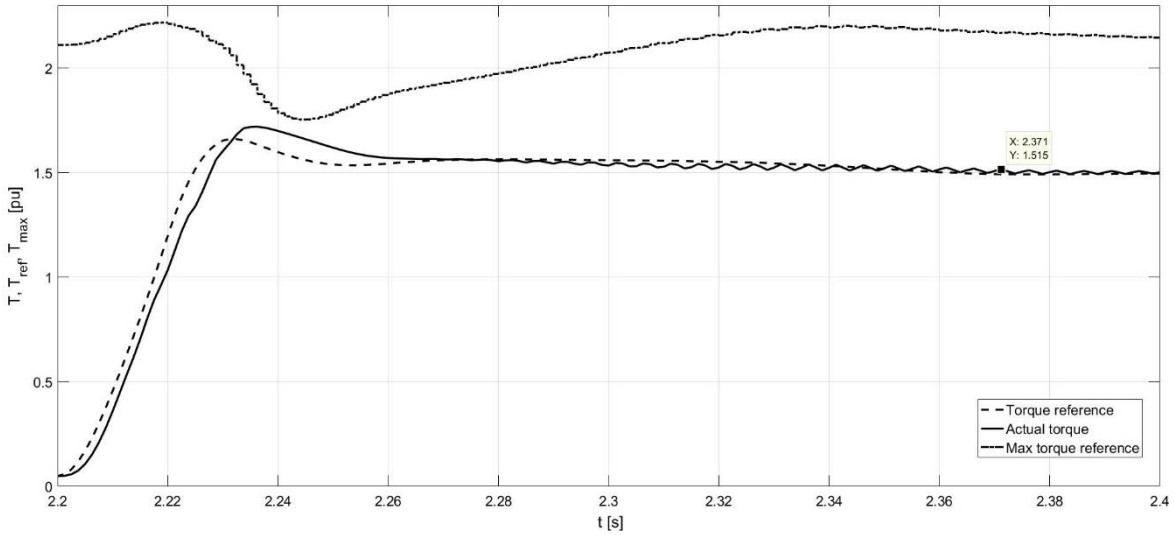

Figure 4.3 – Torque ramp zoomed in for the time period between 2.2 ms and 2.4 ms. The torque transient behavior can be seen more specifically; the load torque rise time is justified to be equal to 20 ms.

As it can be seen from Figure 4.3, the steady state torque value is reached in 171 milliseconds; the overshoot is 14.5%.

The speed transient (Figure 4.4) shows, that the steady state speed value is reached in 148 milliseconds. The speed drop after the torque load application is 2%; there is no overshoot in the speed transient.

The obtained speed and torque steps justify, that the synchronous motor drive model works correctly; the transient time after the load application is reasonable and applicable. Neither torque nor speed steps has fluctuations near the operational level. However, the considered in chapter 3 tuning parameters should also be tested.

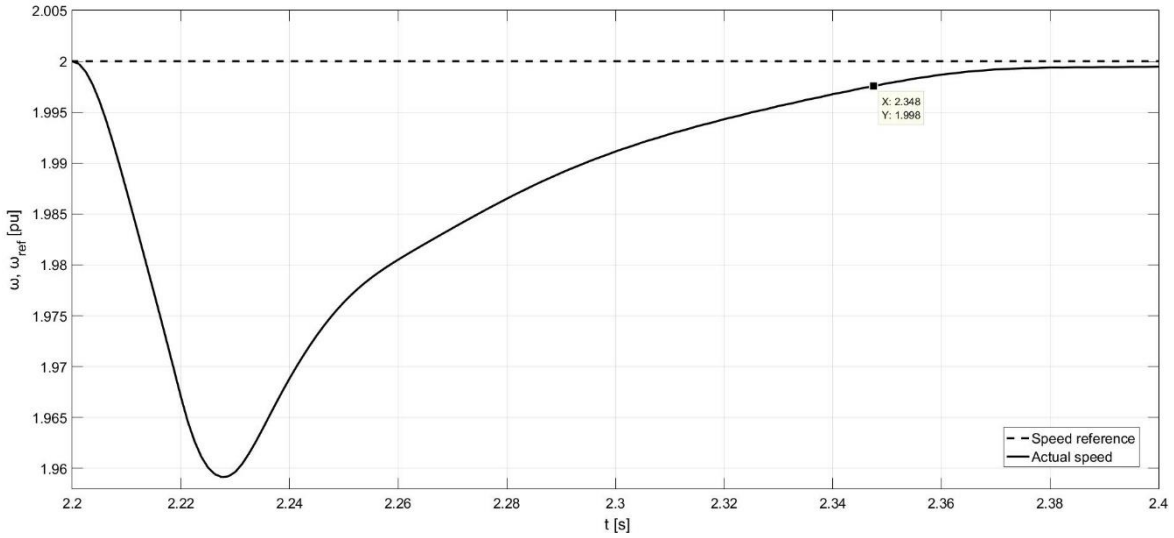

Figure 4.4 – Speed drop due to the load application zoomed in for the time period between 2.2 ms and 2.4 ms. The curve should not be misleading: in the figure the large scale is used to illustrate the transient behavior in detail; the speed drop amounts to only 2%.

In the next paragraph the load torque rise time impact on the drive performance is tested.

Load torque rise time tuning

The torque rise time represents the rapidity of load application. In other words, in most conventional industrial applications one of the crucial requirements is the time, during that the torque reaches its operational value. In processing industry, or in marine applications the load is often applied suddenly and all at once. Thus, the less load rise time can be achieved, the wider is the possible applications field.

In the model, initially the 20 ms load rise time was specified, that means the torque load is increased from the level of 5% to 150%. However, the unity power factor excitation control method does not allow for lower than 20 ms rise time value; for the sake of discussion, the torque load rise time value of 50 ms was tested as well.

The obtained during the simulation torque transient curve is presented in Figure 4.5. As it can be seen from the figure, the torque ramp has smoother slope due to the increased rise time value. Considering the graph specifically, the figure points out that the overshoot is 8%, and the steady state value is reached within 181 ms. By increasing the torque load rise time the overshoot, as well as the speed drop, can be reduced significantly, though the system

rapidity deteriorates proportionally. Furthermore, rather high rise time values are unacceptable from the point of view of possible industrial applications.

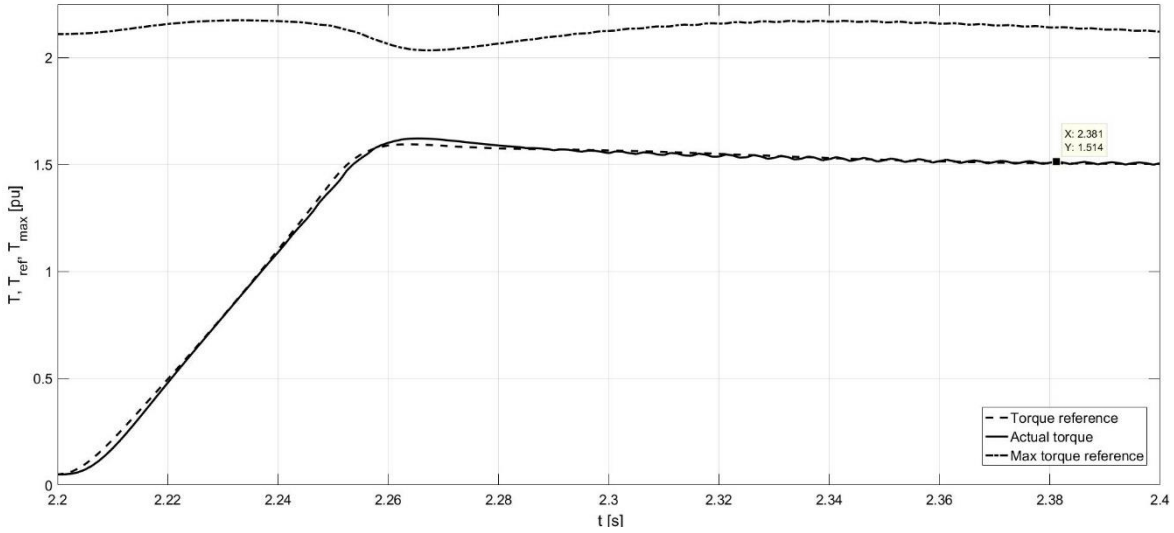

Figure 4.5 – Torque step obtained while testing the torque load rise time equaling 50 ms. Extended fragment.

The experiments justified the control system inability to manage the load rise time below the limit of 20 ms. However, even this limit proves a high level of the drive dynamic performance.

Stator current control tuning

The drive dynamic performance analysis is continued with the further control system development. For this reason, the stator current control tuning as described in paragraph 3.2 is conducted.

During the previous tests, the current controllers were tuned by specifying the currents rise time equaling 5 ms. However, to determine the currents rise time influence, and thus, controllers proportional and integral gains, the values being equal to 1 ms and 7 ms are simulated.

The torque steps obtained during the experiments are presented in Figure 4.6 - 4.7.

Judging by the torque transients obtained during the simulations, a certain trade-off between oscillations suppression and the overshoot reduction should be kept.

As the figures point out, higher rise time value leads to the increased torque overshoot (23%), while smaller rise time value reduces the overshoot, but increased oscillations and the steady state error occur.

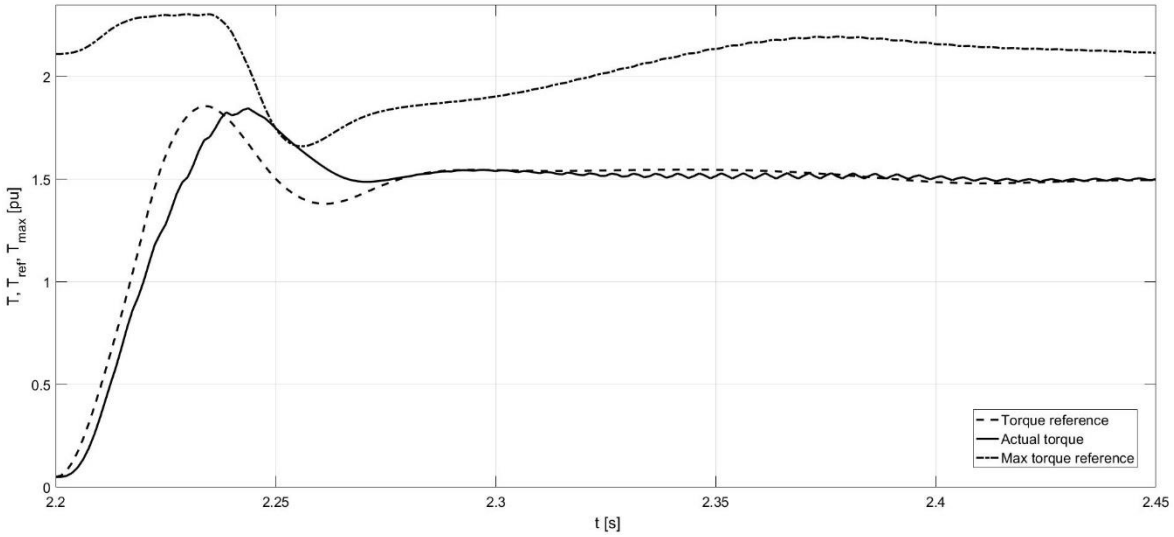

Figure 4.6 – Torque step obtained while testing the stator current rise time equaling 7 ms. Extended fragment.

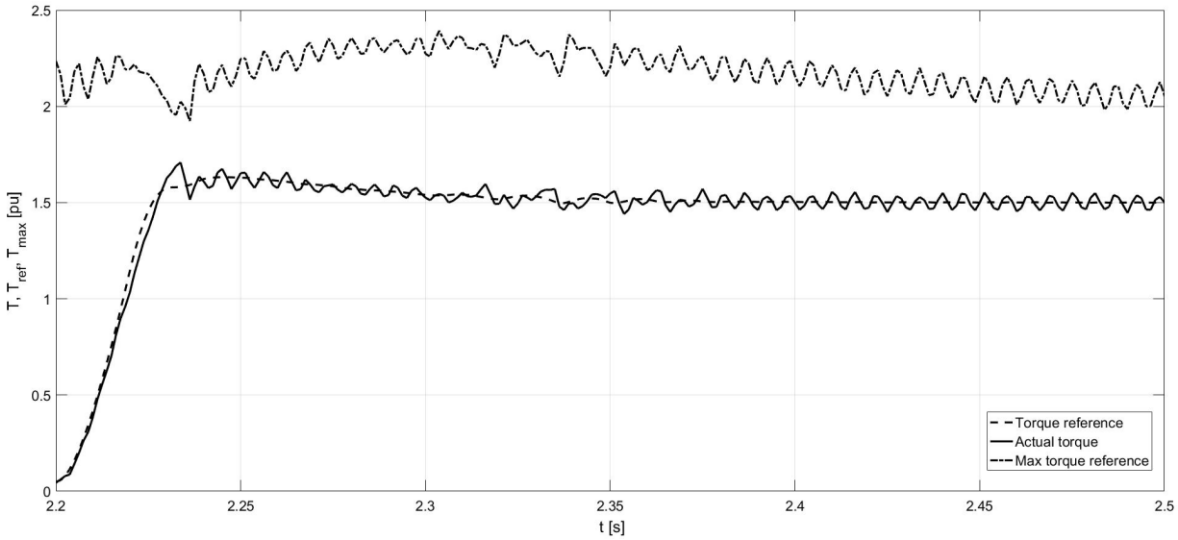

Figure 4.7 – Torque step obtained while testing the stator current rise time equaling 1 ms. Extended fragment.

At this point, the unity power factor excitation control principle was tested thoroughly, with all the tuning parameters discussed in chapter 3 simulated. The tuning combination with the highest dynamic performance level among the simulation experiments comprises the stator

flux linkage reference vector, the load torque rise time value of 20 ms, and the stator currents rise time equaling 5 ms each.

Even though the control system ensures high dynamic performance, the drive can be modified and analyzed further by researching the reaction excitation control method described in paragraph 3.4. The simulation results are presented in the following paragraph.

4.2 Reaction excitation control simulation

In the second set of experiments reaction control is simulated. In accordance with the principle, the power factor is changed from the initial value, that is equal to 0.152 for the investigated drive, to the final working point, where it is amounted to the unity. Besides that, the tuning parameters remain the same as during the unity power factor control simulations.

Stator flux linkage reference vector definition

During the first simulation of the control system based on the reaction excitation control principle the correctness of the stator flux linkage reference vector definition is tested. The load torque and stator currents rise time values are specified by their default values. The obtained torque and speed ramp extended fragments are illustrated in Figures 4.8 – 4.9.

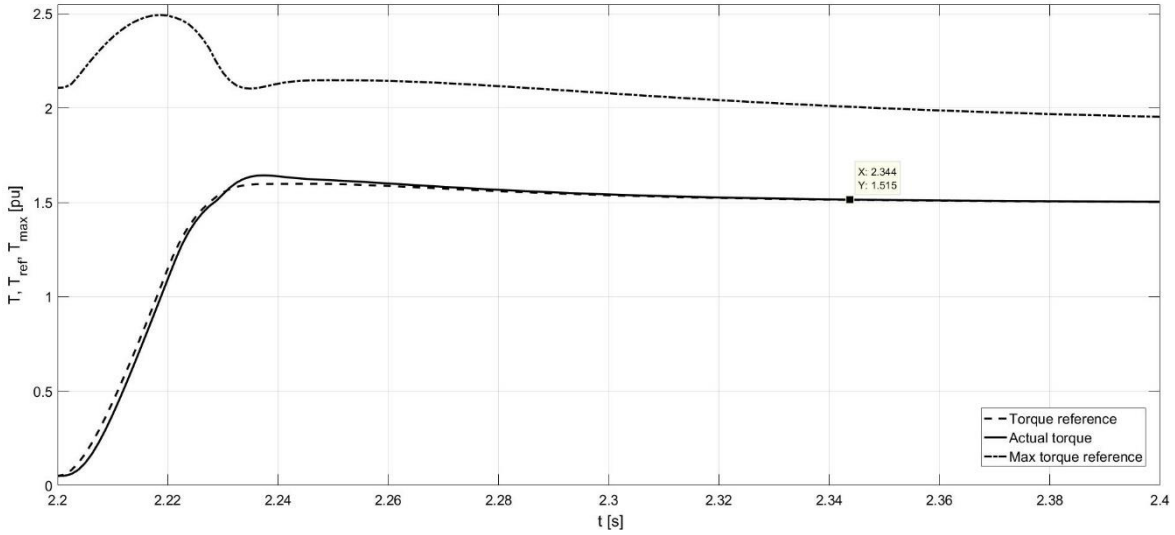

Figure 4.8 – Torque ramp obtained during the simulation. Extended fragment.

The drive performance behavior is similar to the unity power factor one. As Figure 4.8 points out, the steady state error, as well as the torque oscillations near the working point are eliminated; the actual torque value follows the reference curve almost ideally. The steady state torque value is achieved in 0.144 seconds approximately; the overshoot is 9.5%.

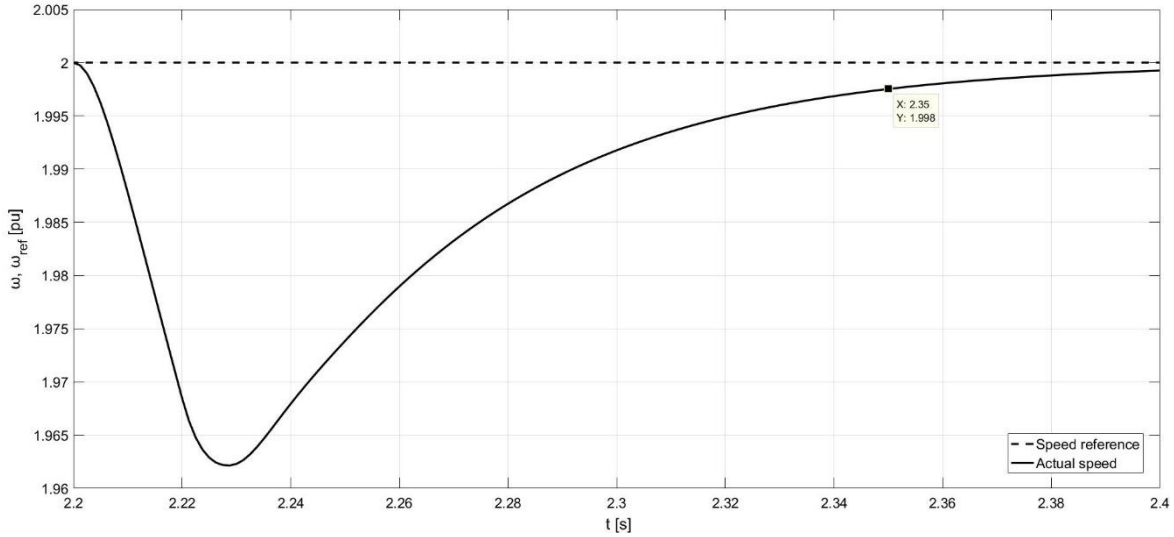

Figure 4.9 – Speed ramp obtained during the simulation.

The speed transient (Figure 4.9) shows, that the steady state speed value is reached in 0.15 seconds. The speed drop after the torque load application is 1.9%; there is no overshoot in the speed transient.

The reaction control performance high quality is justified by the torque and speed transients analysis.

Load torque rise time tuning

During the second simulation, the load torque ramp rise time was changed gradually in order to determine the minimum rise time the drive can manage; reducing the value up to 1 ms, the machine was tested to withstand the rapidly applied torque load.

The torque curve obtained while simulating the load torque rise time of 1 ms is illustrated in Figure 4.10.

As it can be seen from the figure, for the time of 65 ms since the torque application the actual torque does not reach the reference curve; during the time instants from 2.217 and 2.244 the actual and maximum torque reference curves coincide. This feature reflects the torque limiter

performance: the actual torque cannot exceed the maximum available torque level without the synchronism loss. Otherwise, at this working point the load angle would exceed the 90° level, and the machine operation would be stopped to prevent the emergency occurrence. Judging by the torque ramp, the steady state torque value is reached in 126 milliseconds approximately, the overshoot being equal to 16.7%.

In comparison with the previous experiment, the overshoot value is two times higher, however, taking into consideration the torque application rapidity, and the time of the steady state achievement, the drive proved its high performance level even under so rapidly applied load torque.

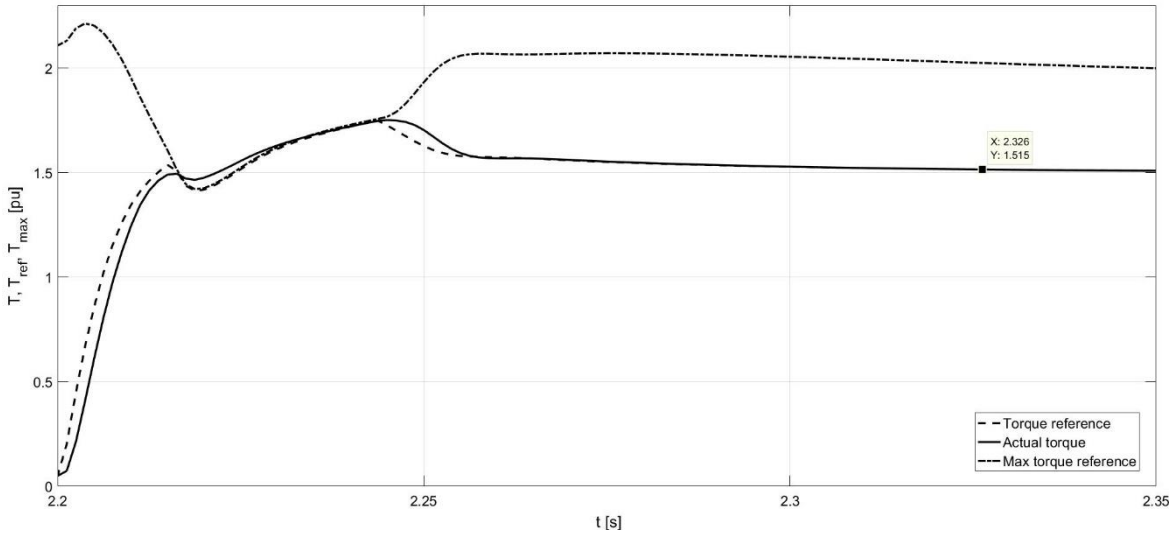

Figure 4.10 – Torque ramp extended fragment. The load torque is applied during 1 ms.

Even though the drive was tested under the severe conditions, the following experiments are continued with the torque load rise time being equal to the initially specified 20 ms.

Stator current control tuning

During the third experiment, the stator currents rise time is changed, and its influence on the drive performance is investigated. For this reason, the rise time values of 1 ms and 7 ms are tested as during the unity power factor control simulation; the results are presented in Figures 4.11 – 4.12.

From the torque ramps, it is seen that no oscillations, or steady state error occur in both cases. The overshoot in case of 1 ms rise time is equal to 8.5%; when the rise time of 10 ms is used,

the overshoot is 10.6%. The time the torque reaches the steady state value of 1.5 pu is the same for both rise time values, and is amounted to 0.144 seconds. However, the reduced rise time provides the offset reduction between the actual and reference torque curves.

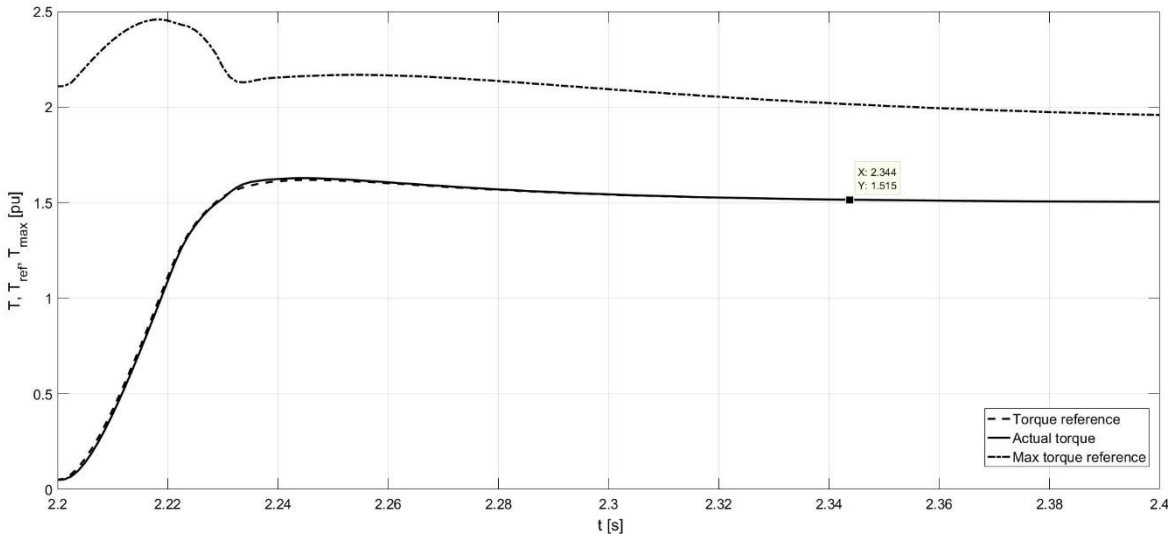

Figure 4.11 – Torque step obtained while testing the stator current rise time equaling 1 ms. Extended fragment.

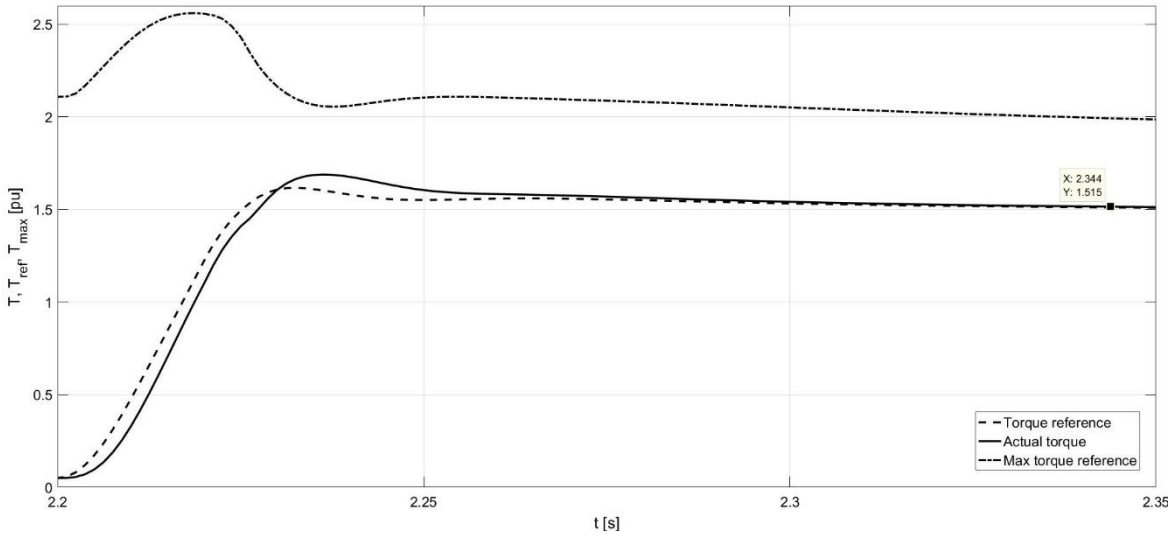

Figure 4.12 – Torque step obtained while testing the stator current rise time equaling 7 ms. Extended fragment.

For this reason, the recommendation to use lower rise time values for the stator current controllers tuning can be given.

Thus, the reaction excitation control principle was simulated, and the tuning parameters affecting the drive dynamic performance were considered and analyzed.
However, the remaining issue to be simulated within the current project is the drive robustness to the internal disturbances. The robustness test results are presented in the following paragraph.

4.3 Robustness analysis

To test the investigated drive robustness to internal disturbances the magnetizing inductances values were reduced by 10% to simulate the saturation phenomena occurrence as discussed in paragraph 3.5. The voltage model based estimator with the current model based correction term introduced in paragraph 3.5 is implemented and used to observe the stator flux linkage actual values, preventing the inaccuracy occurrence due to the inductance parameters elimination from the estimator.
The torque and speed transients under the torque load application are presented in Figure 4.13.

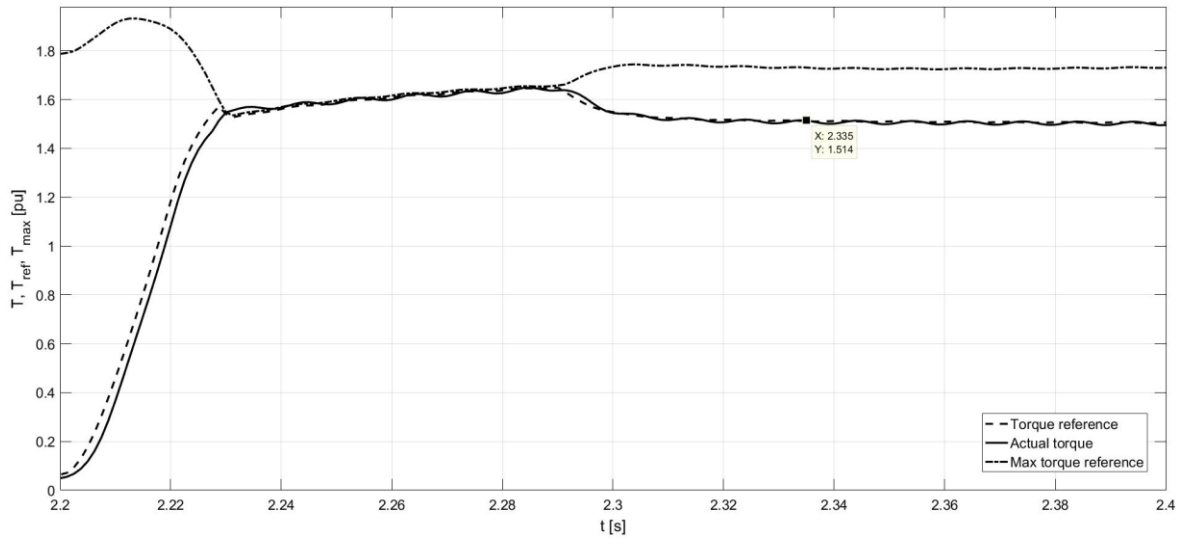

Figure 4.13 – Torque step obtained while testing the drive robustness. Extended fragment.

The torque transient justifies the researched drive robustness. Even though the torque limiter operation is seen for the time period from 2.23 until 2.293, the steady state value with decaying minor oscillations is achieved in 135 ms. The overshoot value is amounted to 9.9%.

As it can be seen from the speed transient (Figure 4.14), the settling time is equal to 115 ms, and the speed drop due to the load applied is 1.95%.

To test more severe conditions, the robustness test was also conducted at the reduced load torque rise time of 1 ms. The torque step illustrated in Figure 4.15 proves the high dynamic performance level even under severe load conditions.

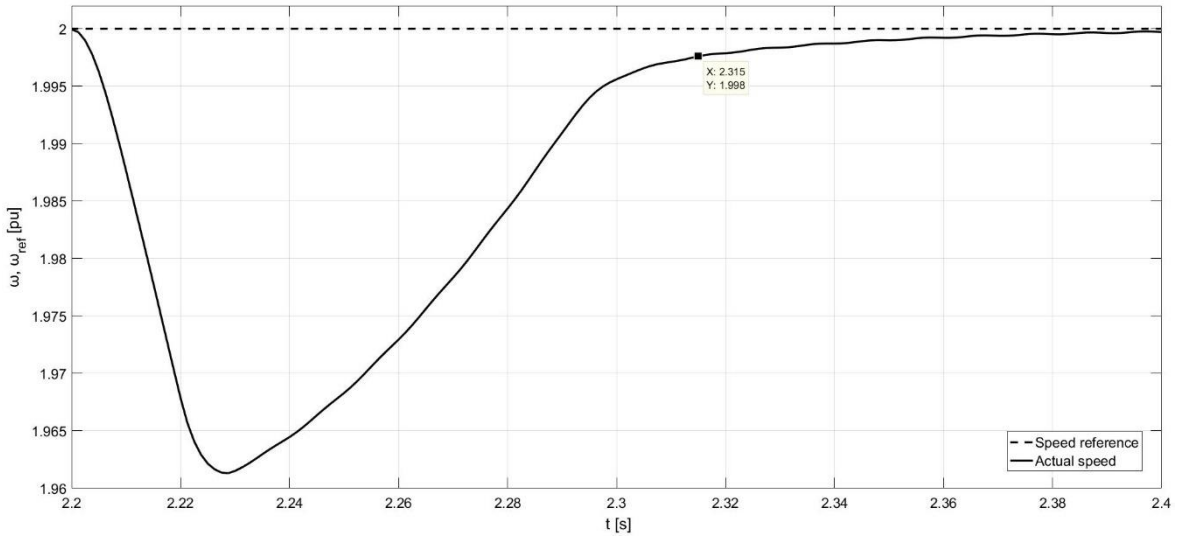

Figure 4.14 – Speed step obtained while testing the drive robustness. Extended fragment.

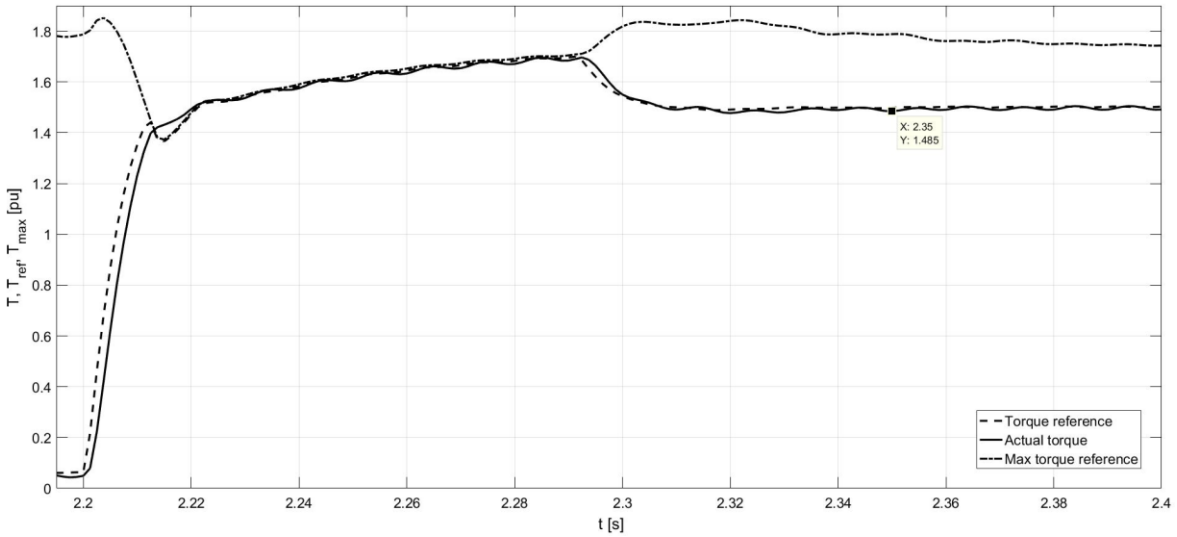

Figure 4.15 – Torque step obtained while testing the drive robustness under severe load conditions (the load torque rise time is equal to 1 ms). Extended fragment.

However, if the magnetizing inductances saturation is assumed to lead to 20% value reduction, the control system is unable to withstand the parameters change.

For this reason, the research in the field of robustness is not enough to judge about the disturbance rejection ability of the investigated drive.

4.4 Results discussion

Judging by the obtained torque and speed transients during the simulations made the following conclusions were made.

The unity power factor technique used in the researched drive has certain limitations. First of all, the load torque rise time is limited by the value of 20 ms; more rapidly applied load destabilizes the control system, the motor synchronism with the power grid is lost, and the drive operation is interrupted. Even though by applying the load of 20 ms rise time, the drive could be considered as a rapid one, the ability of this parameter increase could be a benefit in a number of industrial, and marine applications.

Another drawback of unity power factor control is small oscillations seen at the torque ramps during all the conducted simulations, though the speed transients are insensitive to this minor fluctuations. By increasing the torque load rise time the ripple can be minimized.

The current controllers tuning, i.e. the stator currents rise time has not brought benefit to the drive performance. The decrease in this parameter leads to the increased torque overshoot seen after the load application, while by increasing the currents rise time the torque ripple is also aggravated. The initially used value of 5 ms is the most efficient rise time among the simulated.

The tuning combination with the highest drive performance rate was seen during the first and second simulations, when the only parameter to be changed was the torque load ramp rise time. The further drive performance development was inefficient without the excitation control principle change.

The reaction control principle presented in paragraph 3.4 proved its high performance during the simulations. This excitation control method allows for considerably low load torque rise time values; the simulated rise time of 1 ms did not lead to any failures in the researched drive model. However, decrease in the torque load rise time is accompanied by the corresponding overshoot increase seen at the torque transient.

By reducing the stator currents rise time, the drive performance can be slightly enhanced; the simulated value of 1 ms allows the motor torque to follow the reference torque more precisely.

Judging by the obtained transients, reaction control in comparison with the unity power factor control provides higher dynamic performance level; the measures used are the settling time and the overshoot.

Taking everything into consideration, the most efficient (in terms of the drive performance) combination of the tuning parameters among the simulated is the control system based on the reaction excitation control with the reduced load torque and the stator currents rise time values; the load application rapidity is compensated by the currents rise time.

Conclusion

In the current work the electrically excited synchronous motor drive was investigated. The main topics within the project were field oriented control; the drive performance in the field weakening range; the reaction excitation control method; the drive robustness to the internal disturbances. The investigated drive was tested using the MATLAB Simulink software; the drive model was built using the discrete solver with the fixed step size of one microsecond.

The EESM drive control system was designed on the field oriented control technique. Five low-level controllers were used to control the motor speed, stator flux, excitation, and stator currents; all the control loops were based on PI-controllers. As feedback signals, the stator and excitation currents, as well as the rotor angular velocity were used. The reference values for the controllers were either specified in the lookup tables, or calculated based on the outputs of the other controllers. The current controllers (both stator and excitation) were tuned based on the Internal Model Control (IMC) principle. In accordance with the technique, the controller proportional and integral gains were calculated based on the desired currents rise times; the currents rise time influence on the drive performance was investigated and demonstrated during the simulations.

The drive performance at higher speeds, i.e. at levels exceeding the nominal speed, was achieved by the field weakening implementation. When the maximum available stator voltage level is reached, the following speed increase is impossible without the stator flux linkage reduction, also known as field weakening. In the investigated drive the field weakening operation was implemented by the flux limiter; the speed levels are associated with the corresponding stator flux linkage values following the Faraday`s law: the higher the motor speed, the lower flux should be to keep the induced back emf constant. The stator flux linkage reference vector calculation equations were presented in the report; the drive model simulations proved the reference vector specification correctness.

The excitation control methods were represented by the unity power factor control, and the reaction excitation control methods. The investigated drive simulations showed, that unity power factor control cannot ensure as high dynamic performance as provided by the reaction control principle. As its name suggests, in the unity power factor method the $\cos(\phi)$ value is kept at unity, while reaction control allows to use different power factor values. However, during the drive model simulations in the transients it was demonstrated, that the excitation current at the starting working point is not enough to compensate the stator current in d-axis,

and thus, the conclusion that the reaction excitation control method cannot be used directly from the motor start was made. Instead, the unity power factor excitation control technique was used for the motor acceleration to the speed level of double nominal speed; the reaction excitation control was switched on in the partial load mode at double nominal speed. After the load torque application, the power factor value was changed from the initial value to the unity by linear approximation, and the motor remained in this working mode during the whole operational time. The results obtained during the model simulations verified the theoretical view on the researched control methods.

Robustness is a system stability quality to keep low sensitivity and good disturbance rejection. In the current work, the drive robustness to the internal disturbances was investigated. Since the drive performance was studied in the field weakening range, the motor inductances might be subject to saturation. For this reason, the magnetizing inductances were assumed to have 10% value reduction, and the drive dynamic performance under these conditions was researched. To fulfill the technical requirements to keep insensitivity to the parameters fluctuations, the new flux linkage estimator topology was introduced. Originally, the current mathematical model of the EESM was used to implement the flux linkage estimator. The stator and damper winding flux linkages in dq-axes were estimated based on the machine currents measured. However, the current model estimator has a significant drawback – the estimator equations contain the inductances, that ruin the systems stability in case of wrong parameters assumption. For this reason, the voltage model based estimator was introduced; this mathematical model allowed to eliminate the dependence on the inductances values, what enhanced the control system robustness. However, the flux linkage transients obtained during the simulations showed that such a topology cannot be used from the starting working point. The contradiction was eliminated by implementing the voltage model based estimator with the current model based correction term. The error between the flux linkage values calculated by two models is supplied to the controller, that generates the correction term added to the voltage model result. The high performance of the complicated flux estimator topology was justified during the simulated robustness test with the error in the magnetizing inductances assumed. However, the simulations made demonstrated, that the investigated drive is unable to withstand the parameters change exceeding 10%; further development in the control system is required to keep insensitivity to the internal disturbances and parameters fluctuations. Thus, the conclusion about the drive robustness cannot be made due to the lack of experimental results.

As the project result, the control system with the improved performance was designed and simulated. In the proposed control system the reaction excitation control method, and the improved estimator were implemented; the contribution of the controllers tuning, and the flux linkage reference vector specification was also significant.

Among the possible prospects of development is a total automation of calculations made during the current research; for instance, the stator flux linkage reference vector definition could be implemented as an iterative cycle inside the drive model. The most efficient power factor value used in reaction control for a certain operational point could be determined directly in the model as well. The robustness test conducted within the research was focused only on the internal parameters fluctuations; though, further research and the drive development is required to investigate the drive robustness. However, to make a verdict about the EESM drive robustness, the outer disturbances should be considered as well, e.g. the dynamically changing load.

References

1. Pyrhönen J., Hrabovcová V., Semken R.S. (2016). Electrical Machine Drives Control: An Introduction. 500 p.

2. Pyrhönen, O. (1998). Analysis and control of excitation, field weakening and stability in direct torque controlled electrically excited synchronous motor drives. Research Papers. Dissertation, Lappeenranta University of Technology. ISBN 951-764-274-1.

3. Franklin G.F., Powell J.D., Workman M.L., 1998. Digital control of dynamic systems. 3rd edition. 742 p.

4. Harnefors L., H.-P. Nee, 1998. Model-Based Current Control of AC Machines. Using the Internal Model Control Method. IEEE Transactions on Industry Applications, Vol. 34, No. 1, January/February 1998. p.133-141

5. Vostrov K. (2016). Synchronous machine vector control system development and implementation. Master`s Thesis, Lappeenranta University of Technology.

6. Dai P., Fu F., Fu X., Zong W., Zhou E. (2011). Electrically Excited Synchronous Motor Reduced-Order Flux Observer. In: Wan X. (eds) Electrical Power Systems and Computers. Lecture Notes in Electrical Engineering, vol 99. Springer, Berlin, Heidelberg.

7. X. Wu, G. Tan, M. Liu, H. Li, "Electrically Excited Synchronous Motor Three-Level DTC SVM Control Based on Novel Flux Observer», International Conference on Electrical and Control Engineering (ICECE), 2010, pp. 3689-3692.

8. Y. Zhou and Y. Hu, "A Novel Direct Torque Control for Electrically Excited Synchronous Motor Drives with High Power Factor and Low Ripples in Flux and Torque", IEEE Power Electronics Specialists Conference, 2008, pp. 4752-4756.

9. G. H. B. Foo and X. Zhang, "Robust Direct Torque Control of Synchronous Reluctance Motor Drives in the Field-Weakening Region," in *IEEE Transactions on Power Electronics*, vol. 32, no. 2, pp. 1289-1298, Feb. 2017.

10. D. Beliav, A. Weigner, R. Paes and S. Weigel, "Field oriented control of a synchronous drive," IEEE International Conference on Electric Machines and Drives, 2005., San Antonio, TX, 2005, pp. 957-961.

11. D. Beliaev, E. Ilyin, A. Shatokhin and A. Weinger, "Synchronous drives with field oriented vector control and their industrial implementation," 2009 13th European Conference on Power Electronics and Applications, Barcelona, 2009, pp. 1-10.

12. C. Rossi, D. Casadei, A. Pilati and M. Marano, "Wound Rotor Salient Pole Synchronous Machine Drive for Electric Traction," Conference Record of the 2006 IEEE

Industry Applications Conference Forty-First IAS Annual Meeting, Tampa, FL, 2006, pp. 1235-1241.

13. Kaukonen, J. (1999). Salient-pole synchronous machine modelling in an industrial direct torque controlled drive application. Dissertation Lappeenranta University of Technology, ISBN 951-764-305-5.

14. Pyrhönen O., Niemelä M., Pyrhönen J., Kaukonen J. Excitation control of DTC controlled salient pole synchronous motor in field weakening range. Advanced Motion Control, 1998. AMC '98-Coimbra., 1998 5th International Workshop on, Coimbra, 1998, pp. 294-298.

15. Pyrhönen J., Pyrhönen O., Niemelä M., Luukko J., Kaukonen J., Pohjailainen P.. Direct torque control of synchronous motor drives for dynamically demanding applications. ETEP Vol. 10, No. 5, September/October 2000.

16. ABB Oy. Synchronous motors. High performance in all applications [online document]. [Accessed 26 April 2017]. Available at https://library.e.abb.com/public/.pdf

17. Mohan, N., Undeland, T. M., Robbins, P. (1995). Power electronics: Converters, applications, and design (2nd ed.). New York, NY: John Wiley & Sons.

18. VEM Group. Electrical machines for industry [online document]. [Accessed 08 May 2017]. Available at https://www.vem-group.com/fileadmin/content/pdf

19. C. Lascu, I. Boldea, and F. Blaabjerg, “A modified direct torque control for induction motor sensorless drive”, IEEE Trans. Ind. Appl., vol. 36, no. 1, pp. 122-130, January/February 2000.

20. Niemelä, M. (1999). Position sensorless electrically excited synchronous motor drive for industrial use based on direct flux linkage and torque control. Research Papers. Dissertation, Lappeenranta University of Technology. ISBN 951-764-314-4.